

## The Optical Aurorae of Europa, Ganymede and Callisto

KATHERINE DE KLEER,<sup>1</sup> ZACHARIAH MILBY,<sup>1</sup> CARL SCHMIDT,<sup>2</sup> MARIA CAMARCA,<sup>1</sup> AND MICHAEL E. BROWN<sup>1</sup>

<sup>1</sup>*California Institute of Technology, 1200 E California Blvd, MC 150-21, Pasadena CA 91125, USA*

<sup>2</sup>*Boston University, 725 Commonwealth Ave, Boston MA 02215, USA*

### ABSTRACT

The tenuous atmospheres of the Galilean satellites are sourced from their surfaces and produced by a combination of plasma-surface interactions and thermal processes. Though thin, these atmospheres can be studied via their auroral emissions, and most work to date has focused on their aurora at UV wavelengths. Here we present the first detections of Ganymede’s and Callisto’s optical aurorae, as well detections of new optical auroral lines at Europa, based on observations of the targets over ten Jupiter eclipses from 1998 to 2021 with Keck/HIRES. We present measurements of O I emission at 6300/6364, 5577, 7774 and 8446 Å and place upper limits on hydrogen at 6563 Å. These constitute the first detections of emissions at 7774 and 8446 Å at a planetary body other than Earth. The simultaneous measurement of multiple emission lines provides robust constraints on atmospheric composition. We find that the eclipse atmospheres of Europa and Ganymede are composed predominantly of O<sub>2</sub> with average column densities of  $(4.1 \pm 0.1) \times 10^{14} \text{ cm}^{-2}$  and  $(4.7 \pm 0.1) \times 10^{14} \text{ cm}^{-2}$ , respectively. We find weak evidence for H<sub>2</sub>O in Europa’s bulk atmosphere at an H<sub>2</sub>O/O<sub>2</sub> ratio of  $\sim 0.25$ , and place only an upper limit on H<sub>2</sub>O in Ganymede’s bulk atmosphere, corresponding to H<sub>2</sub>O/O<sub>2</sub> < 0.6. The column density of O<sub>2</sub> derived for Callisto is  $(4.0 \pm 0.9) \times 10^{15} \text{ cm}^{-2}$  for an assumed electron density of  $0.15 \text{ cm}^{-3}$ , but electron properties at Callisto’s orbit are very poorly constrained.

### 1. INTRODUCTION

The tenuous atmospheres of the Galilean satellites Europa, Ganymede, and Callisto are composed of a combination of O<sub>2</sub>, O, H<sub>2</sub>O, and CO<sub>2</sub>, and are ultimately sourced from their surfaces. The detailed compositions of these atmospheres, along with their spatial distributions and temporal variabilities, thus provide information on their surface compositions and on surface modification processes such as sputtering.

Europa’s atmosphere was first detected via the 1356 and 1304 Å multiplets of atomic oxygen in emission using the Goddard High Resolution Spectrograph (GHRS) on the Hubble Space Telescope (HST) (Hall et al. 1995); additional measurements of Europa’s aurora, and a first detection of the same auroral lines at Ganymede, were subsequently made (Hall et al. 1998). The emission was attributed to electron impact dissociative excitation of predominantly O<sub>2</sub> for both Europa and Ganymede, with perhaps some contribution from atomic O especially in the case of Ganymede, on the basis of the ratio of emission between the two multiplets. The strength of the emission lines corresponds to an O<sub>2</sub> atmosphere of  $2.4 \times 10^{14}$ – $14 \times 10^{14} \text{ cm}^{-2}$  at Europa and  $1 \times 10^{14}$ – $10 \times 10^{14} \text{ cm}^{-2}$  at Ganymede, using *Voyager*- and *Galileo*-based estimates for the density and temperature and the exciting electrons (Hall et al. 1995, 1998).

Various mechanisms have been proposed for the production of these tenuous atmospheres. Motivated by an early claim of a 1  $\mu$ bar atmosphere at Ganymede (Carlson et al. 1973), Yung & McElroy (1977) proposed a sublimation-driven water atmosphere that produces a molecular O<sub>2</sub> atmosphere due to photolysis of H<sub>2</sub>O followed by the escape of the lighter hydrogen. However, this model predicts a surface density well above the subsequent *Voyager 1* findings (Broadfoot et al. 1979; Wolff & Mendis 1983). Lanzerotti et al. (1978) proposed that Ganymede’s atmosphere is produced by jovian plasma bombardment, which sputters neutral molecules off the icy surface, and argued that this is a more efficient mechanism for producing O<sub>2</sub> especially at the low end of plausible surface temperatures. Brown et al. (1980) then measured ion sputtering yields as a function of ice temperature, and more recent modeling work has calculated sputtering yields of O<sub>2</sub> and H<sub>2</sub> for Europa (Cassidy et al. 2013) and for icy satellites in general (Teolis et al. 2017). Thermal H<sub>2</sub> and O<sub>2</sub> products do not condense as efficiently as sputtered water molecules, and H<sub>2</sub> readily escapes, leaving O<sub>2</sub> as the primary constituent. Johnson et al. (1981); Johnson et al. (1982) used these experiments to predict that a  $\sim 10^{14}$  cm<sup>-2</sup> atmosphere of O<sub>2</sub> would be sustained at Ganymede and  $\sim 10^{15}$  cm<sup>-2</sup> at Europa, and also calculated an expected  $\sim 2 \times 10^{12}$ – $1 \times 10^{14}$  cm<sup>-2</sup> of H<sub>2</sub>O across the three icy satellites. However, models subsequently showed that O<sub>2</sub> yields from ion sputtering are insufficient to match the observed column densities, unless additional “resputtering” by freshly ionized O<sub>2</sub> augments the flux from Jupiter’s magnetosphere (Ip 1996). Saur et al. (1998) modeled the atmospheric sources and sinks, including plasma deflection, and found that a combination of supra-thermal torus ions and thermal ions sputtering O<sub>2</sub> from the surface could produce a stable atmosphere around the measured column densities, and demonstrated that the re-sputtering mechanism could not contribute a significant amount.

Images of Europa and Ganymede in the UV O I multiplets (1304 and 1356 Å) with HST/STIS have yielded evidence for spatial variations across both satellites (McGrath et al. 2013; Feldman et al. 2000; Roth et al. 2016). For Europa the spatial distribution of emissions exhibits some systematic trends but is still not fully understood. A dusk-dawn asymmetry is observed in both the UV and optical auroral data (Roth et al. 2016; de Kleer & Brown 2019), which is consistent with simulations (Oza et al. 2019) and suggests a thermal role in the production of the O<sub>2</sub> atmosphere (Oza et al. 2018; Johnson et al. 2019). For Ganymede, the aurora appear to behave analogously to Earth’s auroral ovals, whereby electrons are accelerated into the near-surface region along field lines at the open-closed field line boundary (McGrath et al. 2013; Feldman et al. 2000; Eviatar et al. 2001). The oscillation amplitude of the ovals has been used as evidence to support the existence of a subsurface ocean on Ganymede (Saur et al. 2015). The brightness of Ganymede’s auroral spots cannot be matched by models assuming the electron energies and densities at Ganymede’s orbit, requiring either higher electron energies or higher-density, lower-temperature electrons (Eviatar et al. 2001); the higher electron energies are attributed to local acceleration at Ganymede (Eviatar et al. 2001). The uncertainties on the electron population exciting the emissions permit O<sub>2</sub> column densities in the range of  $1 \times 10^{14}$ – $30 \times 10^{14}$  cm<sup>-2</sup> for Ganymede. In contrast, Europa’s auroral emissions are consistent with excitation by thermal magnetospheric electrons and do not require local acceleration (Saur et al. 1998).

Recently, Roth (2021) and Roth et al. (2021) used auroral data sets to independently constrain the atomic O abundance in the atmospheres of Europa and Ganymede by measuring the resonant scattering component of the 1304 Å emission as the satellites passed through Jupiter’s shadow. These data sets put a tight upper limit on the O abundance, which then requires a new mechanism to explain the low 1356/1304 Å ratio (sometimes referred to as  $r_{\gamma}(\text{OI})$ , e.g. (Roth 2021)) on these satellites’ trailing hemispheres. The proposed mechanism is a consistently-present H<sub>2</sub>O atmosphere centered on the trailing hemisphere for Europa and both hemispheres (though 6× denser on the trailing) for Ganymede, which can be produced by sublimation

in the case of Ganymede (as is also predicted on Callisto; Carberry Mogan et al. 2021) and by sputtering combined with sublimation of the fresh deposits of sputtered  $\text{H}_2\text{O}$  in the case of Europa (Roth 2021; Teolis et al. 2017). The derived mixing ratios of  $\text{H}_2\text{O}/\text{O}_2$  over the trailing hemisphere are in the 10 to 30 range for both satellites. The UV lines are significantly more sensitive to  $\text{O}_2$  than  $\text{H}_2\text{O}$ , and observations of H in addition to O, and/or observations of lines with higher intrinsic emission rates following electron impact on  $\text{H}_2\text{O}$ , would strengthen constraints on  $\text{H}_2\text{O}$  presence and abundance.

To date, studies of the auroral emissions of Europa and Ganymede have been conducted almost exclusively in the UV. However, measurements of additional lines at different wavelengths can provide more robust constraints on atmospheric composition, and have the potential to reveal additional processes at work or even new atmospheric constituents. The optical auroral lines have been studied at Io for decades (e.g. Belton et al. 1996; Schmidt et al. in press). On the icy Galilean satellites, whose atmospheres and orbital environments are both less populated than those of Io, the first published detection of the optical aurora was the 6300/6364 Å oxygen emission observed at Europa from HST/STIS and the Keck High Resolution Spectrograph (HIRES) (de Kleer & Brown 2018, 2019). The data supported an  $\text{O}_2$  atmospheric composition and displayed a high level of temporal variability and spatial patchiness on top of an overall asymmetry in the auroral brightness with more emission on the trailing/dusk side, consistent with the UV morphology observed by Roth et al. (2016).

Here we present observations of Europa, Ganymede, and Callisto in Jupiter eclipse, over ten eclipses total between 1998 and 2021, taken with Keck/HIRES. The data cover wavelengths from 5000–9000 Å. We present measurements of the 6300/6364, 5577, 7774 and 8446 Å OI emissions from these satellites. All emission lines listed are detected on at least one occasion, and we present upper limits on dates when a given line is not detected, as well as on  $\text{H}\alpha$  6563 Å on all dates. The observations and data reduction procedures are described in Section 2. The model used to interpret the data is expanded from that of de Kleer & Brown (2018) and is described in Section 3, including the MCMC retrieval algorithm. The derived auroral brightnesses are presented and discussed in Section 4, and conclusions are summarized in Section 5.

## 2. OBSERVATIONS AND DATA REDUCTION

Observations of Europa, Ganymede, and Callisto in Jupiter eclipse were obtained on 4, 4, and 2 occasions, respectively, between 1998 and 2021 using the HIRES instrument (Vogt et al. 1994) on the Keck I telescope at the summit of Maunakea in Hawaii. Observations in eclipse remove the reflected sunlight component which would otherwise overwhelm the signal from the visible-wavelength aurora. One eclipse observation of Ganymede is from 1998, which utilized HIRES pre-upgrade when it had a single CCD and less extensive spectral coverage. Table 1 lists the observing parameters for each of these ten nights. The observing sequence typically consisted of 300-second integrations on the satellite while in eclipse, alternated with offsets to a nearby sunlit pointing satellite to check positioning and recenter if needed. The total on-target integration time used in the analysis for each observation is given in Table 1.

The HIRES post-upgrade three CCD mosaic covers wavelengths from roughly 5000–9500 Å with our observing set-up. The echelle and cross-disperser angles were chosen to ensure that the lines of interest did not fall in the gaps between orders. A slit width of 1.722" was used to cover the entire satellite, resulting in a spectral resolution of approximately 24 000. Slit lengths of 7" and 14" were alternately used; a longer slit length increases the amount of sky available for sky subtraction but results in overlap between the orders at short wavelengths.

**Table 1.** Observing parameters.

Date [UTC]	Time [UTC]	Target	$t_{\text{int}}$ [min]	Diam. [arcsec]	CML <sup>a</sup> [°W]	BG <sup>b</sup>	Avg. Sep. <sup>c</sup>	Notes
1998-11-15	05:56–08:55	Ganymede	40	1.63	10–16	1.5	2.2	
2018-03-22 <sup>d</sup>	12:27–14:15	Europa	50	0.91	350–357	38	0.7	Poor weather
2018-06-15	07:10–08:54	Ganymede	20	1.58	7–11	18	1.0	
2021-05-20	13:40–15:05	Europa	40	0.87	345–351	5.4	1.2	
2021-06-08	12:48–15:17	Ganymede	85 <sup>e</sup>	1.55	348–353	2.1	2.1	
2021-06-21	13:05–15:15	Europa	60	0.96	345–354	5.7	0.9	
2021-07-04	14:13–15:25	Callisto	25	1.54	349–350	1	3.7	
2021-07-16	10:12–11:39	Europa	50	1.03	348–354	14	0.6	
2021-09-26	09:05–11:03	Callisto	20	1.58	5–9	1.7	2.4	Poor weather
2021-10-01	04:55–08:19	Ganymede	70	1.70	7–14	2.3	1.3	Poor weather

<sup>a</sup>Central meridian longitude, or sub-observer longitude.

<sup>b</sup>Sky background level measured near 6300 Å, relative to a measured 21 electrons s<sup>-1</sup> arcsec<sup>-2</sup> background in the Callisto observations taken July 4, 2021.

<sup>c</sup>Average angular distance of the target from Jupiter’s limb in units of Jupiter radii.

<sup>d</sup>Previously published in [de Kleer & Brown \(2018\)](#).

<sup>e</sup>Some infrared orders are removed during averaging due to additional contamination; total integration times were 70 minutes for 7774 Å and 60 minutes for 8446 Å.

To correct for cosmic rays, we used the Laplacian cosmic-ray identification method L.A.Cosmic ([van Dokkum 2001](#)) as implemented in the Astropy-affiliated package `ccdproc` using the methodology described in [McCully et al. \(2018\)](#). We then bias-subtracted, flat-fielded and gain-corrected all science images. We used the sharp edges in the flat-field to identify the boundaries of the individual echelle orders which we used to rectify each order. For the wavelength calibrations we used thorium-argon arc lamp lines to calculate a wavelength solution for each echelle order by fitting third-degree polynomials. We also corrected for airmass extinction using the wavelength-dependent magnitude attenuation appropriate for the summit of Maunakea derived by [Buton et al. \(2013\)](#). To subtract the background, we calculated a characteristic, normalized spatial profile along the slit in the area immediately around the emission line, excluding pixels contained within an aperture covering the target satellite. We then fit this profile and a constant term using ordinary-least-squares to subtract the background from each echelle order.

To calibrate each observation from electrons s<sup>-1</sup> bin<sup>-1</sup> to rayleighs (R), we calculated an expected spectral surface brightness for Jupiter’s central meridian using its absolute reflectivity ([Woodman et al. 1979](#)) and a solar reference spectrum scaled to the Jupiter-Earth distance at the time of the observations. We then calculated the total number of electrons per second per arcsecond from Jupiter at each auroral wavelength, which provides a direct conversion from electrons to photons. To extract the target surface brightness, we calibrate the data using the apparent angular size of the target disk and the Jupiter flux calibration described above, then fit a Gaussian model and integrate it over a window of  $\pm 1$  Å around the line center (or each line center for a multiplet emission). We calculate brightnesses from both individual frames and an average of all frames.

The reduced and calibrated spectra in the vicinity of each measured emission line on each date are shown in Figure 1.

In order for a detection to be reported instead of an upper limit, the following conditions must be met:

1. The fitted surface brightness indicates a detection at the  $2\sigma$ -level or better,
2. The emission line is centered at the expected Doppler-shifted wavelength given the line-of-sight motion of the target,
3. The emission is localized along the slit, and
4. The spectrum passes a visual inspection to ensure no false detections are reported due to poor background subtraction or other systematic contributions.

For cloudy or non-photometric nights, we report whether or not a detection was made but do not give quantitative measurements or upper limits due to the uncertainty on the flux calibration. Figure 1 color-codes these cases as described in the caption.

### 3. ANALYSIS

#### 3.1. Emission Model

All observations were made with the target satellites in Jupiter eclipse, which removes any ambiguity about the relative roles of photo-excitation vs. electron excitation. Our model assumes that all auroral emissions are produced by electron impact direct excitation or dissociative excitation of oxygen-bearing species. The model includes the parent species O, O<sub>2</sub>, H<sub>2</sub>O and CO<sub>2</sub>. The strength of the observed emission lines is a function of the satellite's atmospheric composition and density, and the density and energy distribution of the incident electrons. Our model is adapted from that described in [de Kleer & Brown \(2018\)](#) and uses experimentally-derived emission cross-sections. The electron energies and temperatures for Europa's orbital location are taken from [Bagenal et al. \(2015\)](#) and are derived from *in situ* measurements; we use an electron density of 160 cm<sup>-3</sup> with Maxwellian-distributed energies, with 95% of the electron population centered at 20 eV and 5% centered at 250 eV. Note that older observational studies, and modeling papers that interpret these observations, used an electron density 4× lower (e.g. [Hall et al. 1995, 1998](#); [Roth et al. 2016](#); [Vorburger & Wurz 2021](#)), and column densities from these works need to be scaled down by a factor of 4 for comparison with our results and with other more recent work ([de Kleer & Brown 2018, 2019](#); [Roth 2021](#)). The model of [Oza et al. \(2019\)](#) uses an electron density of 70 cm<sup>-3</sup>, intermediate between the two values used in other work.

The electrons at Ganymede's orbit were similarly observed by *Voyager* to be composed of two populations, with a cold population at 30–60 eV and a hot population at 200 eV constituting 10% of the total number density of 3–10 cm<sup>-3</sup> ([Sittler & Strobel 1987](#)). However, [Eviatar et al. \(2001\)](#) demonstrate that the electron populations at Ganymede's orbit are insufficient to explain the brightness of the UV aurora and postulate that the aurora are excited by electrons locally accelerated to 100 eV. We follow these and other previous authors in adopting a Maxwellian distribution of electron energies centered at 100 eV, with an electron density of 20 cm<sup>-3</sup> (though note that some modeling work has used a higher density of 70 cm<sup>-3</sup>; [Leblanc et al. 2017](#)). An electron density of 20 cm<sup>-3</sup> is consistent with recent *in situ* measurements from the Ganymede *Juno* fly-by, which took place one day prior to our 2021-06-08 Ganymede eclipse observation ([Kurth et al. 2022](#)). Although the electron properties are uncertain and therefore the derived column densities should be viewed



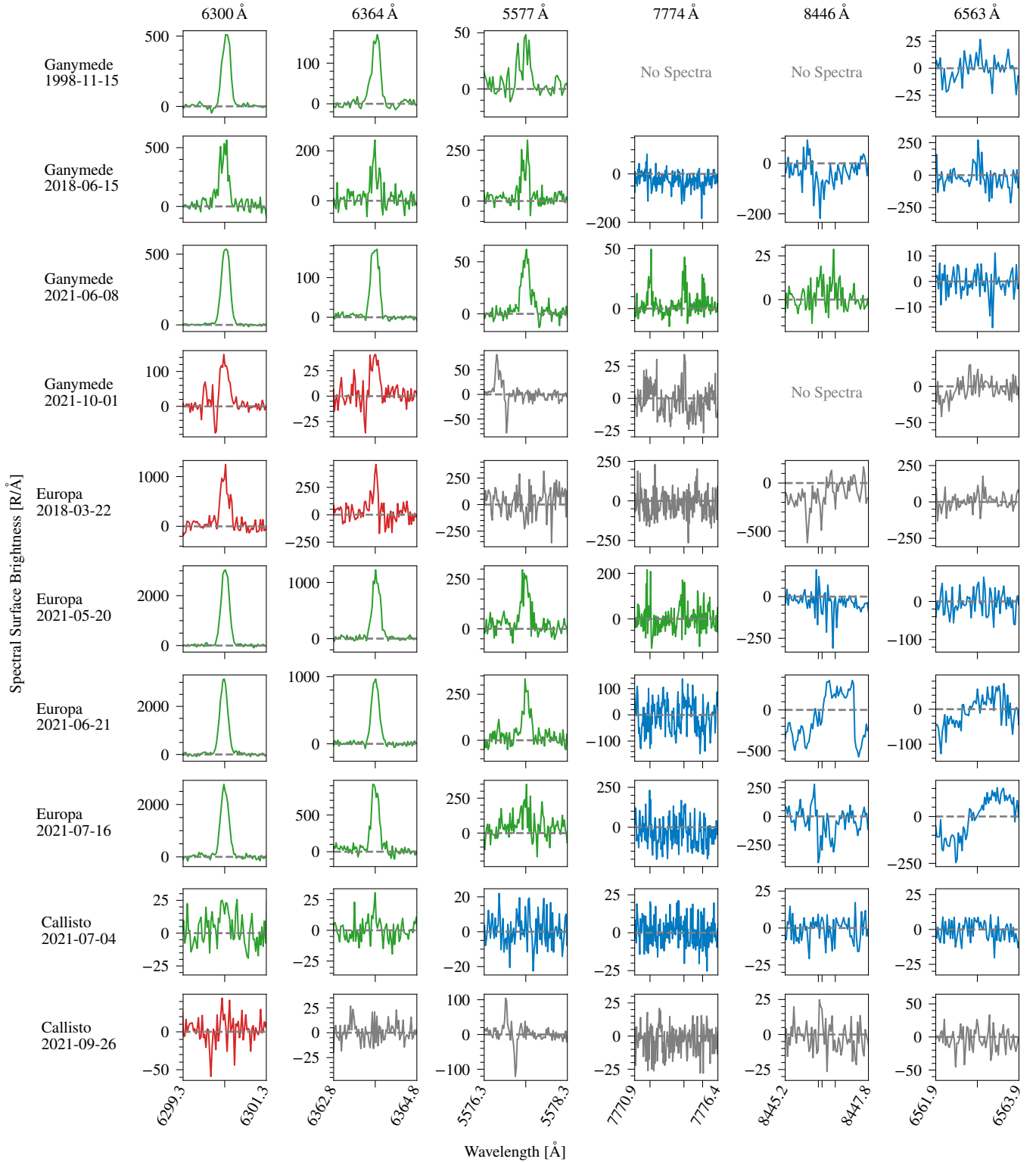


**Figure 1.** Average spectra centered on each emission line discussed in this paper on each night of observation. All spectra are reported in  $R \text{ \AA}^{-1}$  divided by the angular size of the target. Green spectra are detections with calibrated line strengths; red spectra indicate cloudy nights where a detection is made but no quantitative measurement is reported; blue spectra indicate upper limits are reported; and black spectra are non-detections where no upper limit is reported due to non-photometric conditions. Ticks along the horizontal axis shows the location of the center of the emission line(s) and the numbers on the bottom row indicate the wavelength boundaries of each plot in that column. For single emission lines, the boundaries are  $\pm 1 \text{ \AA}$  from the line center. For triplet lines the boundaries are  $-1 \text{ \AA}$  from the shortest wavelength and  $+1 \text{ \AA}$  from the longest wavelength. All emission lines arise from atomic oxygen except for hydrogen at  $6563 \text{ \AA}$  (which is not detected).

with caution, the ratios between emission lines do not change substantially with adopted electron properties and the relative abundances of different species is therefore robust to this uncertainty.

For Callisto, information on the electron energies and densities is even more limited. *Voyager* measured an electron density of  $0.1\text{--}1.0\text{ cm}^{-3}$  at Callisto's orbit (Belcher 1983), while *Galileo* found  $0.01\text{--}1.0\text{ cm}^{-3}$  depending on plasma sheet distance (Kivelson et al. 2004). The electron temperature estimates from the above works range from  $35\text{--}200\text{ eV}$ , with a supra-thermal population. We adopt a density of  $0.15\text{ cm}^{-3}$  at  $35\text{ eV}$  following Belcher (1983). This is the same electron density adopted by Cunningham et al. (2015), but they included a hot population at  $1.5\text{ keV}$  constituting 27% of their total population. The cross-section measurements do not extend to this energy, but we test adding a hot population at the same ratio at either  $250\text{ eV}$  and  $1.5\text{ keV}$  (extrapolating the cross-sections beyond the measurement energies), and find that derived column densities change by up to  $\pm 30\%$  depending on the electron energies. This is well within the uncertainty in the overall electron densities, so we neglect the hot electron population in our modeling.

In addition to extending the model to Callisto, we update the model of de Kleer & Brown (2018) by adding  $\text{CO}_2$  as a parent molecule. Emission cross-sections for electron impact dissociative excitation of  $\text{CO}_2$  are not available for several of the UV/optical O I emission lines, and for  $\text{CO}_2$  our model therefore includes only emission from the  $\text{O}(^1\text{S})$ ,  $\text{O}(^3\text{S})$  and  $\text{O}(^5\text{S})$  states at  $5577$ ,  $1304$  and  $1356\text{ \AA}$  respectively. We adopt the emission cross sections for  $\text{O}(^1\text{S})$  recommended by Itikawa (2002), which are based on the measurements of LeClair & McConkey (1994). We adopt the cross sections for  $\text{O}(^3\text{S})$  from Ajello (1971), but note that their measurements disagree with those of Mumma et al. (1972) even after revised normalization of the latter (Itikawa 2002), and the cross sections are consequently uncertain at the  $\sim 10\%$  level over most electron energies and even higher at the low end of the electron energy distribution. Ajello (1971) also measured the emission from the  $\text{O}(^5\text{S})$  state at  $1356\text{ \AA}$ . Their emission cross sections are presented relative to those of  $1304\text{ \AA}$  and are therefore limited by the propagated uncertainties from the  $\text{O}(^3\text{S})$  measurements. Additionally, the authors note that the  $1356\text{ \AA}$  emission is a lower limit since the  $\text{O}(^5\text{S})$  atom may acquire excess kinetic energy during dissociation beyond the thermal velocity. The limitations on the above measurements, and the lack of measurements for other emission lines, highlights the need for future lab measurements of these cross-sections for interpretation of aurora at  $\text{CO}_2$ -containing atmospheres throughout the solar system.

Our updated auroral model now also includes the O I emissions at  $7774$  and  $8446\text{ \AA}$  from parent molecules  $\text{O}$ ,  $\text{O}_2$  and  $\text{H}_2\text{O}$ . Both emission features are triplets that are produced by the atomic oxygen transitions  $(3p\ ^5\text{P}) \rightarrow (3s\ ^5\text{S}^\circ)$  and  $(3p\ ^3\text{P}) \rightarrow (3s\ ^3\text{S}^\circ)$  respectively. Their radiative cascades to ground produce the well known  $1356\text{ \AA}$  and  $1304\text{ \AA}$  UV lines, and so the cascade contributions into these UV lines is simply equal to the  $7774$  and  $8446\text{ \AA}$  brightnesses in Rayleigh units. The cross-sections for both emissions following electron impact on  $\text{O}_2$  are taken from Schulman et al. (1985); on  $\text{H}_2\text{O}$  from Beenakker et al. (1974) following the recommendation of Itikawa & Mason (2005); and on  $\text{O}$  from the excitation cross-sections recommended by Laher & Gilmore (1990), which are based on the measurements of Gulcicek et al. (1988) and Gulcicek & Doering (1987).

The methodology of this emission model relies on some implicit assumptions that warrant brief discussion. First, the approach assumes that all emissions are optically thin. Lines with the strongest Einstein A coefficients saturate first in their curve of growth and  $1304\text{ \AA}$  has the strongest transition probability herein. The brightness of the HST/COS resolved  $1304\text{ \AA}$  triplet at Ganymede matches the optically thin ratio of 5:3:1 (Roth et al. 2021). Locally, Ganymede's emissions are bright relative to the other satellites, which assures opacity effects are negligible overall. A second assumption is that electrons remain warm enough to excite all lines at all altitudes; neutral collisions could cool magnetospheric electrons below the various

thresholds to excite the different emissions. Cooling rates in Earth’s thermosphere are dominated by vibrational excitation of  $O_2$  near  $1 \times 10^8 \text{ cm}^{-3}$  (Pavlov & Berrington 1999), a density expected only very near the surface. A third assumption is negligible collisional quenching of long-lived forbidden transitions. With a lifetime of 134 s (Wiese et al. 1996),  $O(^1D)$  can be collisionally depopulated before radiating. Thermal  $O_2$  gas quenches  $O(^1D)$  at a rate of  $5 \times 10^{-11} \text{ cm}^3\text{s}^{-1}\text{molecule}^{-1}$  (Streit et al. 1976) and so the critical density where  $O_2$  quenches atoms before radiative decay is  $1.5 \times 10^8 \text{ cm}^{-3}$ —again, a negligible effect over the atmospheric columns.

Table 4 gives the modeled emission rate coefficients for the UV and optical emission lines given the relevant electron energies for Europa, Ganymede, and Callisto. Table 5 gives the corresponding emission line ratios for comparison with the observations.

### 3.2. Retrievals of atmospheric composition

We use the emission model described in Section 3.1 to find the best-fit atmospheric column densities for each satellite and date of observation. The model atmosphere is composed of O,  $O_2$ , and  $H_2O$ , and the free parameters in the fits are the disk-integrated column densities of each of these constituents.  $CO_2$  is considered but is ultimately not included in the fits because the cross-sections are unavailable at all but one of the optical lines. The modeled auroral emissions are fit to the measurements and upper limits of the four oxygen transitions (at 5577, 6300/6364, 7774 and 8446 Å) and  $H\alpha$  (6563 Å). An MCMC algorithm is employed to obtain the joint probability distribution of the three atmospheric constituents and hence obtain the most accurate uncertainties on the free parameters. We use the `emcee` Python implementation (Foreman-Mackey et al. 2013) of the affine-invariant ensemble sampler for Markov chain Monte Carlo (MCMC) described by Goodman & Weare (2010). An example output of the MCMC algorithm is shown in Figure 8. In our results we present our final model with uncertainties; upper limits are presented when a species is found to be present at the  $< 2\sigma$  level. In the Appendix we also report the single maximum likelihood model for each observation.

The strongest constraints on atmospheric composition come from simultaneous measurements that cover the largest range of emission lines. The atmospheric retrievals on data from a single observation have the advantage that all measurements are simultaneous. However, numerous measurements have also been made of the UV auroral lines (e.g., McGrath et al. 2013; Roth et al. 2016). We therefore also retrieve the atmospheric composition using the average measurements of auroral emissions at each transition, including past UV measurements.

For the optical transitions, the values in the average fits are averaged over the two dates for each satellite that had good observing conditions and low scattered light (i.e. 1998-11-15 and 2021-06-08 for Ganymede and 2021-05-20 and 2021-06-21 for Europa; see Table 1). For the UV transitions at Europa, we use values of  $40 \pm 4$  and  $80 \pm 8$  R for the 1304 and 1356 Å emissions respectively, based on 19 observations summarized in Roth et al. (2016). Roth (2021) also present measurements of the UV emissions from the subjovian hemisphere in and out of eclipse that are about half the average value cited above. While these data are a closer match to the viewing geometry of our observations, Roth (2021) show that the aurora are very similar in and out of eclipse, and we adopt the average values rather than the subjovian values because in the case of Europa the time variability seems to be dominated by the plasma sheet distance and stochastic variability rather than hemispheric trends. Using the UV eclipse measurements instead of the average UV measurements in our modeling provides a much worse fit.

The situation is different for Ganymede, where the interactions between Ganymede’s magnetic field and Jupiter’s magnetosphere result in distinct auroral differences between the hemispheres (McGrath et al. 2013).



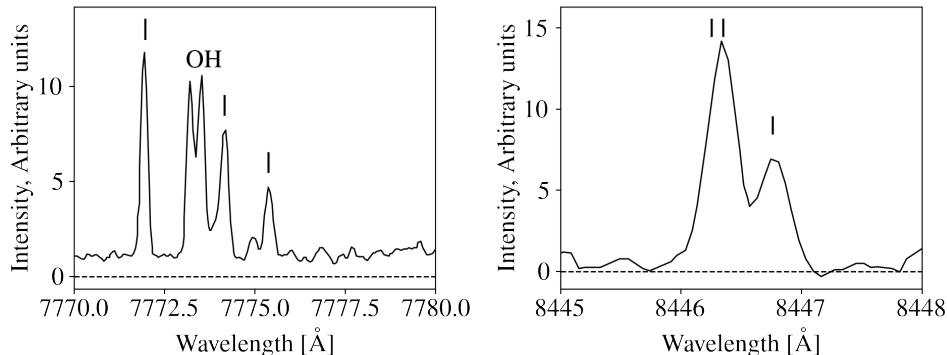


**Figure 2.** Spectrum covering the 7774 and 8446 Å emissions from Earth’s atmosphere, obtained with Keck/HIRES. Figure adapted from [Slanger et al. \(2004\)](#).

In this case, we use the average of the two available subjovian UV measurements, giving values of  $15 \pm 2$  and  $36 \pm 2$  R for the 1304 and 1356 Å emissions respectively ([Roth et al. 2021](#)). While one of these measurements was made in eclipse and one in sunlight, the values are almost identical between the two. Averaging the leading, trailing, and sub-jovian hemisphere measurements from that work gives higher values of  $23 \pm 1$  and  $46 \pm 1$  R, which provide a worse fit when the retrievals are run jointly with the optical data.

Ly- $\alpha$  emission has also been detected on both satellites; on Europa, a value of  $70 \pm 26$  R was found based on two off-limb averages ([Roth et al. 2014a](#)). However, the authors note that these emissions may originate from an extended H cloud around Europa rather than directly from H<sub>2</sub>O dissociation. At Ganymede, the H<sub>2</sub>O-sourced Ly- $\alpha$  emission level predicted by [Roth et al. \(2021\)](#) of 200 R would be inseparable from spatial variations in the surface reflections ([Roth et al. 2021](#); [Alday et al. 2017](#)). We therefore do not include Ly- $\alpha$  values in our average fits; including upper limits would not affect the fits because our H $\alpha$  upper limits provide a much more stringent constraint on H<sub>2</sub>O as a parent molecule because of the smaller uncertainties due to observing in eclipse.

#### 4. RESULTS & DISCUSSION

We report detections of O I emission at 6300/6364, 5577 and 7774 Å at Europa and Ganymede, and additionally 8446 Å at Ganymede only, as well as a detection of 6300/6364 Å emission at Callisto. These constitute the first detections of these lines at any of the icy Galilean satellites, with the exception of the recent measurements of 6300/6364 Å at Europa ([de Kleer & Brown 2018, 2019](#)), and also the first detections of 7774 and 8446 Å emission at a planetary body other than Earth. An Earth spectrum covering these emissions obtained with Keck/HIRES from [Slanger et al. \(2004\)](#) is shown in Figure 2 for context. Emission from these lines has also been modeled at Mars and Venus (e.g. [Bougher et al. 2017](#); [Borucki et al. 1996](#); [Gronoff et al. 2008](#)), but is not strong enough to have been detected to date. 7774 Å emission was reported in an experiment to detect lightning on Venus ([Hansell et al. 1995](#)), but non-detection by a dedicated instrument aboard *Akatsuki* suggests this was spurious ([Lorenz et al. 2019](#)).

The 6300/6364 Å emission is seen in every observation of both targets, while 5577 Å emission is seen on several but not all dates. [Cassidy et al. \(2008\)](#) proposed electron-excited Na could explain Europa’s eclipsed emission in the 2000–10 500 Å wavelength range (clear filter) during *Cassini*’s Jupiter flyby. While the foreground Na nebula from Io hinders our ability measure auroral Na, eclipsed O emissions are more than an order of magnitude brighter than the Na D lines at 5890 and 5896 Å and thus a more viable explanation for the broadband *Cassini* measurement. The 7774 and 8446 Å detections at Ganymede are shown in Figure 3.

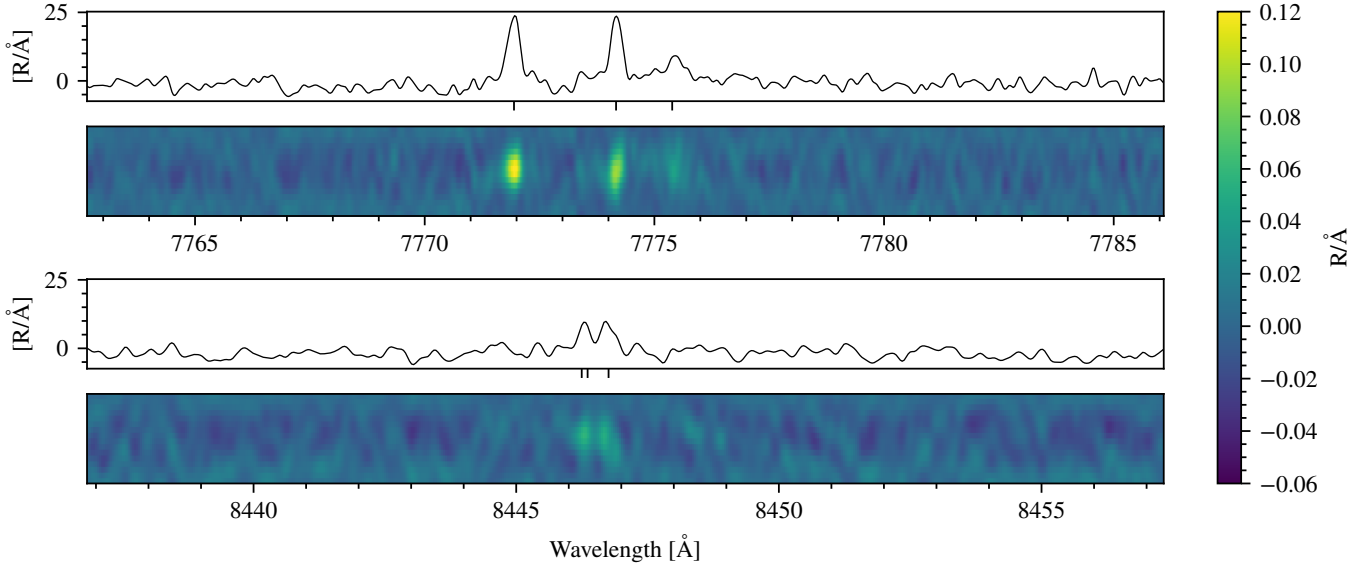


**Figure 3.** Detections of 7774 and 8446 Å OI emission at Ganymede. For each emission, the lower panel shows a calibrated, background-subtracted image of the spectrum so it can be seen that the emission is localized along the slit (vertical axis), while the upper panel shows the spectrum summed across spatial bins containing the localized emission. The vertical ticks between the panels indicate the locations of the Doppler-shifted emission wavelengths for each transition. Each spectrum has been smoothed with a Gaussian kernel to enhance the features relative to the background.

The detection of 6300 and 6364 Å emission at Callisto is shown in Figure 4. The sole previous measurement of Callisto’s oxygen atmosphere was attributed to photo-dissociation of O<sub>2</sub> (Cunningham et al. 2015) and so the emission we report here in shadow constitutes the first definitive detection of Callisto’s electron-excited aurora at any wavelength.

Table 2 provides the disk-averaged surface brightnesses (or  $2\sigma$  upper limits) of Europa, Ganymede, and Callisto on each observation and for every measured emission line. For poor weather nights, when flux calibration was not reliable, we only report whether or not each line is detected. Table 3 presents the best-fit atmospheric composition for Europa and Ganymede for each observation, as well as the best-fit composition based on the optical and UV lines averaged across several dates of observation. Note that the exact values of column density are subject to uncertainty due to the poorly-constrained density of the electrons exciting the emissions, which vary by a factor of a few depending on the study (e.g. Bagenal et al. 2015; Bagenal & Dols 2020; Hall et al. 1995). However, the relative contribution from different molecules to the emissions is robust to this uncertainty since it is constrained by the ratio between emission at different wavelengths (given in Table 5). The modeled and measured brightnesses of all emission lines are shown in Figures 5 and 6 and presented in detail in the Appendix in Table 6.

For Europa, we find that the atmosphere is dominated by O<sub>2</sub> with a column density of  $3.7\text{--}4.1 \times 10^{14} \text{ cm}^{-2}$ . The accurate reproduction of several line ratios via dissociative excitation of O<sub>2</sub> effectively rules out the possibility of an atomic atmosphere proposed by Shemansky et al. (2014), and the column density of atomic oxygen is constrained to be  $< 1 \times 10^{13} \text{ cm}^{-2}$ . Our models tentatively ( $2.4\sigma$ ) indicate the presence of H<sub>2</sub>O at a column density of  $1.2 \pm 0.5 \times 10^{14} \text{ cm}^{-2}$ . Our derived O<sub>2</sub> column density is within the range found by past UV observations; the average brightness at 1356 Å found by Roth et al. (2016) corresponds to an average column density of  $3.75 \times 10^{14} \text{ cm}^{-2}$  after converting from the  $40 \text{ cm}^{-3}$  electron density used in their

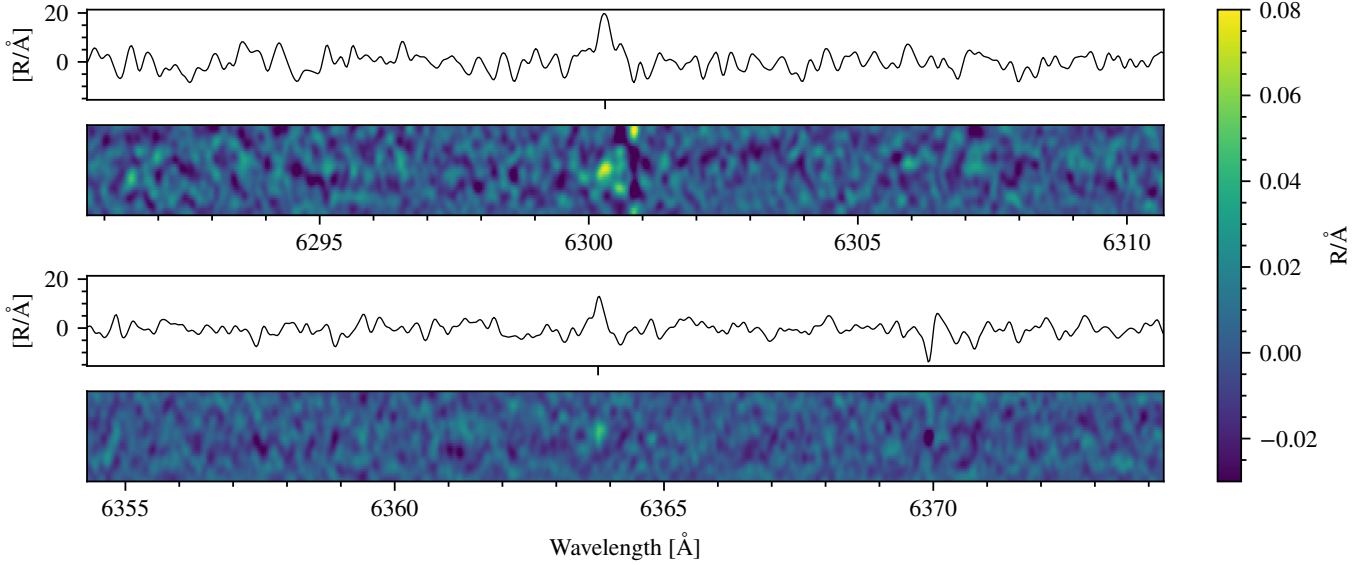


**Figure 4.** Detections of 6300 and 6364 Å O I emission at Callisto. For each emission, the lower panel shows a calibrated, background-subtracted image of the spectrum so it can be seen that the emission is localized along the slit (vertical axis), while the upper panel shows the spectrum summed across spatial bins containing the localized emission. The vertical ticks between the panels indicate the locations of the Doppler-shifted emission wavelengths for each transition. Each spectrum has been smoothed with a Gaussian kernel to enhance the features relative to the background. In the 6300 Å case, the bright points near the top and bottom of the slit just to the right of Callisto are residual from the subtraction of Earth’s 6300 Å, which is Doppler-shifted relative to the target.

calculation to the  $160 \text{ cm}^{-3}$  used in ours. Our upper limit on O of  $< 1 \times 10^{13} \text{ cm}^{-2}$  is similarly consistent with the upper limit of  $6 \times 10^{12} \text{ cm}^{-2}$  derived from UV eclipse observations (Roth 2021). However, our tentative detection of  $\text{H}_2\text{O}$  at  $1.2 \pm 0.5 \times 10^{14} \text{ cm}^{-2}$  is a factor of 10 below the estimated  $\text{H}_2\text{O}$  column density derived from the two UV lines by Roth (2021); this difference is explored in Section 4.1.

For Ganymede, we find that the atmosphere is dominated by  $\text{O}_2$  with a column density of  $3.2 \times 10^{14}$ – $4.8 \times 10^{14} \text{ cm}^{-2}$ , and place an upper limit on O of  $3 \times 10^{13} \text{ cm}^{-2}$ . This upper limit is consistent with the upper limit of  $2 \times 10^{12} \text{ cm}^{-2}$  derived from UV eclipse observations (Roth et al. 2021), although the column density we find for  $\text{O}_2$  is somewhat higher than the  $2.8 \times 10^{14} \text{ cm}^{-2}$  adopted by these authors in their modeling (using the same electron density as in our model:  $20 \text{ cm}^{-3}$ ). We also place an upper limit on  $\text{H}_2\text{O}$  of  $3 \times 10^{13} \text{ cm}^{-2}$ . This is lower by a factor of  $\sim 100$  than the  $\text{H}_2\text{O}$  abundance inferred by Roth et al. (2021). Water in Ganymede’s atmosphere is discussed in more detail in Section 4.1.

These derived  $\text{O}_2$  column densities roughly match predictions by exosphere modeling work for Europa and Ganymede in eclipse (Oza et al. 2019; Leblanc et al. 2017), although we note that the model predictions are for zenith columns whereas our observations are disk-integrated and likely dominated by the tangent column at the limb.

The best-fit models for individual nights occasionally find a contribution from O or  $\text{H}_2\text{O}$ , which could be physically meaningful or could simply be a reflection of the high uncertainty arising from performing retrievals on low signal-to-noise data from individual eclipses. For Ganymede on 2018-06-15, the sky background level was anomalously high (see Table 1) and the inference of  $\text{H}_2\text{O}$  should be viewed with skepticism despite the high mathematical significance. For Europa on 2021-06-21, the contribution from O is marginal (at the  $2.3\sigma$  level), though the data quality is good from this night.

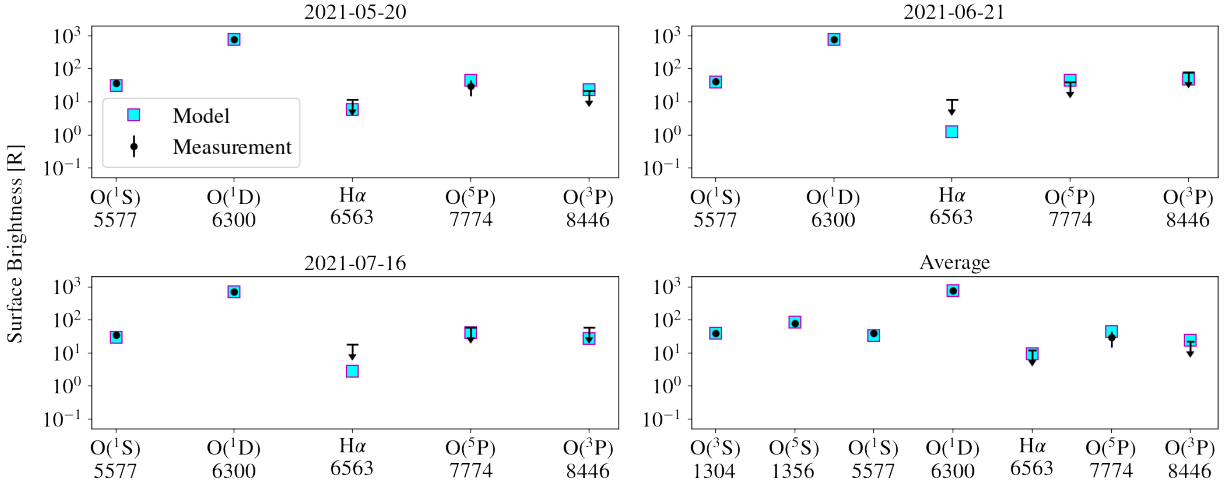


**Figure 5.** Measured auroral emissions along with the best-fit atmospheric model for Europa for each date of observation and for the average auroral emissions including past UV measurements (Roth et al. 2016).

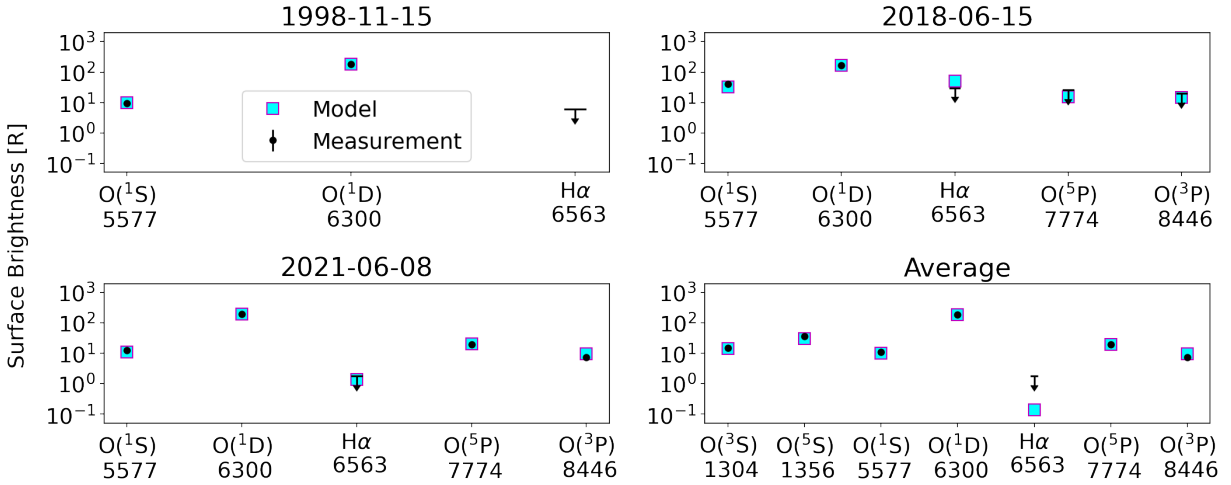


**Figure 6.** Measured auroral emissions along with the best-fit atmospheric model for Ganymede for each date of observation and for the average auroral emissions including past UV measurements (Roth et al. 2021).

For Callisto, the detection of only one excited O I state (6300/6364 Å), combined with the lack of past electron-excited UV detections, limits the complexity of models that can be fit to the data. Using a model that assumes a pure  $O_2$  atmosphere and an electron density at Callisto of  $0.15 \text{ cm}^{-3}$ , we find a column density of  $4.0 \pm 0.9 \times 10^{15} \text{ cm}^{-2}$ , which matches very well with the  $4.0 \times 10^{15} \text{ cm}^{-2}$  inferred from a UV measurements for which the excitation was attributed to photoelectrons (Cunningham et al. 2015). Callisto will be discussed further in Section 4.3.

#### 4.1. $H_2O$ -dominated atmospheres on Europa and Ganymede?

**Table 2.** Measured auroral surface brightnesses and upper limits [R].<sup>b</sup>

Satellite/Date	6300 Å O( <sup>1</sup> D)	6364 Å O( <sup>1</sup> D)	5577 Å O( <sup>1</sup> S)	7774 Å O(3p <sup>5</sup> P)	8446 Å O(3p <sup>3</sup> P)	6563 Å H $\alpha$
<b>Ganymede</b>						
1998-11-15	139 $\pm$ 3	42.9 $\pm$ 1.7	9.2 $\pm$ 1.6	—	—	< 6
2018-06-15	127 $\pm$ 7	36 $\pm$ 5	41 $\pm$ 4	< 26	< 20	< 30
2021-06-08	147.6 $\pm$ 1.5	45.0 $\pm$ 1.0	12.5 $\pm$ 0.6	20 $\pm$ 2	7.3 $\pm$ 1.4	< 1.8
2021-10-01 <sup>c</sup>	<i>detected</i>	<i>detected</i>	—	—	—	—
Average	143 $\pm$ 2	44 $\pm$ 1	11 $\pm$ 1	20 $\pm$ 2	7.3 $\pm$ 1.4	—
<b>Europa</b>						
2018-03-22 <sup>a,c</sup>	<i>detected</i>	<i>detected</i>	—	—	—	—
2021-05-20	573 $\pm$ 14	190 $\pm$ 7	37 $\pm$ 4	30 $\pm$ 15	< 22	< 12
2021-06-21	613 $\pm$ 12	176 $\pm$ 6	42 $\pm$ 5	< 40	< 80	< 12
2021-07-16	547 $\pm$ 14	170 $\pm$ 8	35 $\pm$ 8	< 60	< 60	< 18
Average	593 $\pm$ 9	183 $\pm$ 4	40 $\pm$ 3	30 $\pm$ 15	—	—
<b>Callisto</b>						
2021-07-04	6.1 $\pm$ 1.7	3.3 $\pm$ 1.2	< 2	< 8	< 4	< 3
2021-09-26 <sup>c</sup>	—	—	—	—	—	—

<sup>a</sup>Previously published in [de Kleer & Brown \(2018\)](#).

<sup>b</sup>2 $\sigma$  upper limits; we require a measurement to be at or above the 2 $\sigma$  level to claim a detection.

<sup>c</sup>On poor weather nights when it was not possible to flux-calibrate the data, we report only whether a given line is detected.

Recently, [Roth \(2021\)](#) and [Roth et al. \(2021\)](#) postulated H<sub>2</sub>O-dominated atmospheres on the trailing hemispheres on Europa and Ganymede. This claim is based in part on an observed 1356/1304 Å ratio that is lower for both satellites on the trailing hemisphere than on the leading hemisphere. While this difference had previously been attributed to a greater O abundance on the trailing hemisphere ([Roth et al. 2016](#); [Molyneux et al. 2018](#)), the new observations included eclipse measurements of the subjovian hemisphere, permitting a stronger upper limit on the column density of O by placing a direct constraint on the contribution to 1304 Å from resonant scattering by O.

Our observations are all made in eclipse and therefore image the subjovian hemisphere. In the case of Europa, our upper limit for O of  $\sim 1 \times 10^{13}$  cm<sup>-2</sup> (see Table 2) is consistent with the upper limit of  $6 \times 10^{12}$  cm<sup>-2</sup> derived by [Roth \(2021\)](#). However, our best-fit value for H<sub>2</sub>O,  $1.2 \pm 0.5 \times 10^{14}$  cm<sup>-2</sup>, is a factor of 10 lower than the disk-averaged H<sub>2</sub>O abundance of  $\sim 1 \times 10^{15}$  cm<sup>-2</sup> found by [Roth \(2021\)](#) for the sunlit trailing hemisphere. Note that while the column densities presented here depend on the assumed electron properties, we have adopted the same electron properties as used by [Roth \(2021\)](#) and [Roth et al. \(2021\)](#), so the factors by which the derived column densities differ between studies are not sensitive to uncertainty in electron density and are only weakly sensitive to uncertainty in electron temperature. Similarly, while the absolute abundances of species derived from our modeling depends on electron density, the relative abundances do not and are therefore not subject to uncertainty on this parameter.



**Table 3.** Best-fit model atmospheres<sup>a</sup>.

Satellite/Date	Column Density [ $\times 10^{14} \text{ cm}^{-2}$ ]		
	O <sub>2</sub>	O	H <sub>2</sub> O
<b>Europa</b>			
2021-05-20	$4.0 \pm 0.1$	$< 0.4$	$< 0.9$
2021-06-21	$3.7 \pm 0.2$	$1.8 \pm 0.8$	$< 0.8$
2021-07-16	$3.7 \pm 0.2$	$< 1.2$	$< 1.1$
Average <sup>b</sup>	$4.1 \pm 0.1$	$< 0.1$	$1.2 \pm 0.5$
<b>Ganymede</b>			
1998-11-15	$4.5 \pm 0.1$	$< 3$	$< 0.6$
2018-06-15	$3.2 \pm 0.3$	$< 8$	$16 \pm 3$
2021-06-08	$4.8 \pm 0.1$	$< 0.8$	$< 0.5$
Average <sup>b</sup>	$4.7 \pm 0.1$	$< 0.3$	$< 0.3$
<b>Callisto</b>			
2021-07-04	$40 \pm 9$	—	—

<sup>a</sup>For the following assumed electron parameters, as described and referenced in the text: Europa  $n_e = 160 \text{ cm}^{-3}$  with 95% Maxwellian-distributed in energy about 20 eV and 5% about 250 eV; Ganymede  $n_e = 20 \text{ cm}^{-3}$  Maxwellian-distributed about 100 eV; Callisto  $n_e = 0.15 \text{ cm}^{-3}$  Maxwellian-distributed about 35 eV.

<sup>b</sup>Average atmospheric compositions are based on fits to the average optical and UV brightnesses across all available dates of observation, as described in Section 3.2.

The presence of H<sub>2</sub>O in our modeling is only indicated at the  $2.4\sigma$  level and only after averaging datasets together with the UV; for individual nights, we find only upper limits on H<sub>2</sub>O, in the  $0.8 \times 10^{14}$ – $1.1 \times 10^{14} \text{ cm}^{-2}$  range. For all UV and optical oxygen lines except  $5577 \text{ \AA}$ , the emission rates are at least  $10\times$  higher for O<sub>2</sub> than for H<sub>2</sub>O, so that these lines are not strongly sensitive to H<sub>2</sub>O (see Table 4). However, for  $5577 \text{ \AA}$  the emission rates are comparable between the species. This line, combined with H $\alpha$ , therefore provide the strongest constraints on water abundance. In particular, the H<sub>2</sub>O disk-integrated column density from Roth (2021) would produce 70 R of emission at H $\alpha$ , compared to the  $2\sigma$  upper limit of 12 R from our Europa observations, in addition to predicting O I line ratios inconsistent with the optical and UV lines.

To determine whether an atmosphere containing O, O<sub>2</sub>, H<sub>2</sub>O is preferred over an O<sub>2</sub>-only atmosphere, we fit the data using both the three-species model and the O<sub>2</sub>-only model and find that the fit is only marginally better when all three species are included. Given the lack of strong preference for the H<sub>2</sub>O-containing model and the fact that H<sub>2</sub>O is only preferred by our average fits (and only at  $2.4\sigma$ ), and not on individual nights, we consider the detection of Europa’s H<sub>2</sub>O at all to be tentative in our data. Moreover, we strongly rule out a water abundance of  $2.5 \times 10^{14} \text{ cm}^{-2}$  or higher, or alternatively an H<sub>2</sub>O/O<sub>2</sub> ratio above 0.5, on the eclipsed sub jovian hemisphere.

For Ganymede, our observations on the two nights that had clear sky conditions as well as low Jupiter scattered light conditions (see Table 1) place an upper limits on  $\text{H}_2\text{O}$  of  $3 \times 10^{13} \text{ cm}^{-2}$ , or a maximum  $\text{H}_2\text{O}/\text{O}_2$  ratio of 0.06. In contrast, the modeled ratio for the center trailing hemisphere from the UV data was found to be 12–32 and for the leading hemisphere was found to be 2–5 (Roth et al. 2021), with the disk-averaged ratios a factor of a few lower. This  $\text{H}_2\text{O}$  abundance contributed 1 R to the disk-averaged 1304 Å emission but should contribute 23 R and 46 R to the optical emission at 5577 Å and 6563 Å respectively, both of which are strongly ruled out in our observations.

There are several differences between the optical and UV observations that may be relevant to these different results, in particular the low  $\text{H}_2\text{O}/\text{O}_2$  ratios ( $<1$ ) derived from our optical eclipse data of both satellites, and the much higher ratios of 10–30 determined for the trailing hemispheres in the UV.

First, our observations were made with the targets in shadow while the UV observations were made with the targets in sunlight. For an  $\text{H}_2\text{O}$  atmosphere sustained by sublimation, the column density should be lower in eclipse due to the lower surface temperature. Leblanc et al. (2017) modeled Ganymede’s  $\text{H}_2\text{O}$  exosphere in eclipse and calculated a 4 orders-of-magnitude collapse, from a peak column density in the  $10^{14}$  to  $10^{16} \text{ cm}^{-2}$  range. However, in such a case the UV auroral brightnesses would also be lower in eclipse than in sunlight, whereas the observed brightnesses of both satellites’ aurora are comparable in and out of eclipse (Roth 2021; Roth et al. 2021). A sublimation atmosphere that partially collapses in eclipse therefore cannot reconcile the UV and optical datasets. For Europa, even the  $\text{O}_2$  atmosphere is modeled to drop by an order of magnitude in eclipse (Oza et al. 2019), which is not consistent with the UV observations either.

The observations also differ in that we target the subjovian hemisphere, while the UV-derived  $\text{H}_2\text{O}$  abundances were highest on the trailing hemispheres of both Europa and Ganymede. For Europa, the UV line ratio is also just as low, and hence as inconsistent with pure  $\text{O}_2$ , on the subjovian hemisphere as it is on the trailing hemisphere (Roth 2021). The past UV data and our optical results together are therefore hard to reconcile with the presence of significant O or  $\text{H}_2\text{O}$  on Europa, which seems to require a new explanation for the low 1356/1304 Å ratio at least on the subjovian hemisphere.

For Ganymede, the UV line ratio is higher on the subjovian hemisphere than either leading or trailing (Roth et al. 2021) and is consistent with pure  $\text{O}_2$ . The difference between the UV and optical data for Ganymede can thus be attributed to an  $\text{H}_2\text{O}$  atmosphere that is only present on the leading/trailing hemispheres, and not on the subjovian, regardless of whether it is sunlit or eclipsed.

Given the clear differences between hemispheres on both moons, it may be that the upper limit derived for O on the subjovian hemispheres is not applicable to the trailing hemispheres, and hence that both O and  $\text{H}_2\text{O}$  remain candidates to explain the low UV ratio on the trailing hemispheres. If atomic O is primarily a product of electron-impact dissociation of  $\text{O}_2$ , it is similarly predicted to be most abundant on the center of the trailing hemisphere for Europa (Cassidy et al. 2013), so either species would produce a 1356/1304 Å ratio that increases from center to limb of the trailing hemisphere as observed.

A sputtered  $\text{H}_2\text{O}$  atmosphere has also been proposed for both satellites (Johnson et al. 1981). For Ganymede, recent modeled sputtered  $\text{H}_2\text{O}$  column densities are in the  $10^{11}$  to  $10^{13} \text{ cm}^{-2}$  range, while modeled sublimated column densities are on the order of  $\sim 10^{16} \text{ cm}^{-2}$  (Marconi 2007; Leblanc et al. 2017; Vorburger et al. 2022). Such sublimated column densities are ruled out in our data, but the expected sputtered column densities are low enough to be below our detection limits. For Europa, sublimated  $\text{H}_2\text{O}$  should be roughly two orders of magnitude lower than for Ganymede based on their surface temperatures, while sputtered  $\text{H}_2\text{O}$  is limited to  $10^{13} \text{ cm}^{-2}$  as for Ganymede (Feistel & Wagner 2007; Plainaki et al. 2013; Schematovich et al. 2005; Smyth & Marconi 2006). Both predictions are near our detection limits, so we cannot

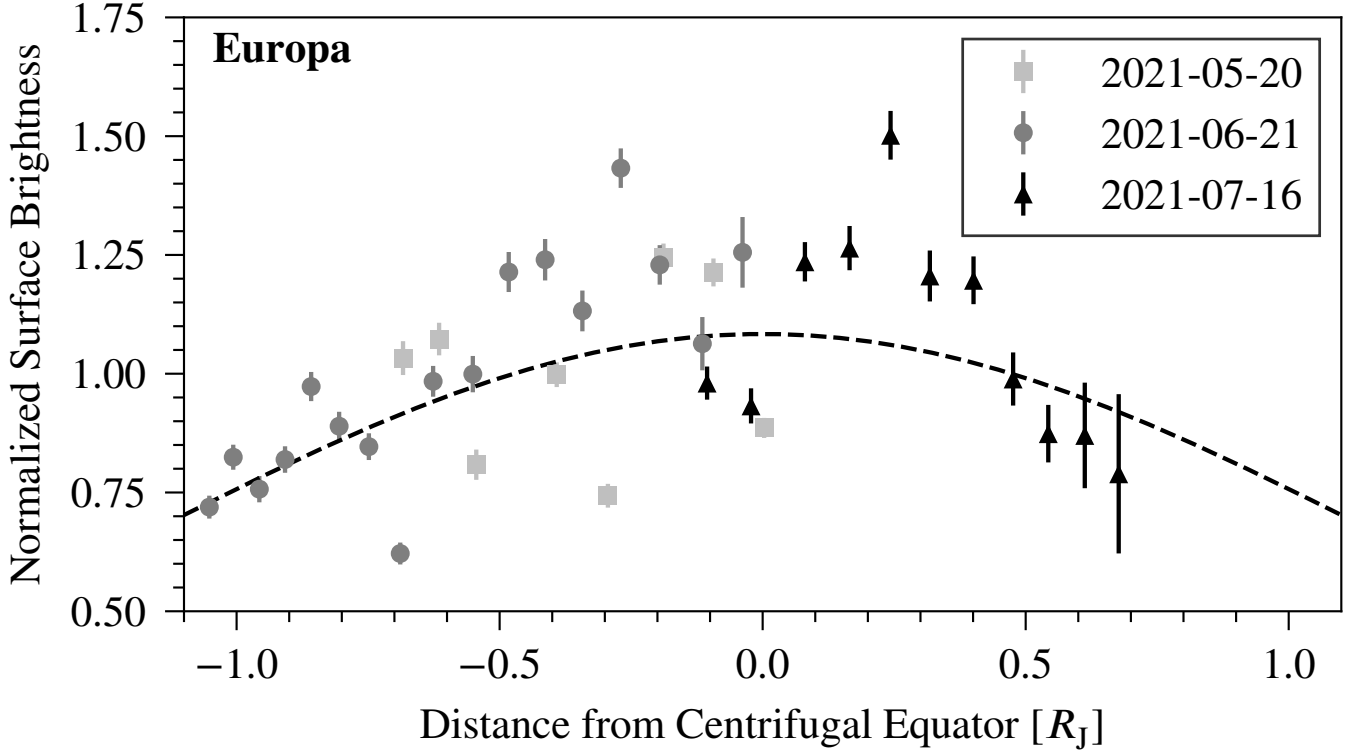


**Figure 7.** Brightness of Europa’s aurora as a function of plasma sheet distance during each observation. Each observation has been normalized to its average. The dashed curve corresponds to a scale height of  $1.67 R_J$ .

provide strong constraints on a potential sputtered  $H_2O$  atmosphere. The expected sputtering production is also longitudinally variable. For Ganymede, [Leblanc et al. \(2017\)](#) show that the  $H_2O$  sputtering production should be highest on the leading hemisphere due to the magnetic field geometry, while for Europa [Cassidy et al. \(2013\)](#) show that sputtering rate of all species is highest on the trailing hemisphere.

#### 4.2. Time-variability of Europa’s aurora

While Ganymede’s aurora are produced by complex interactions between the incoming plasma and Ganymede’s magnetic field, Europa’s auroral brightness should be a more straight-forward product of the local electron density and the column density of species in its atmosphere. In the UV, the aurora are found to vary by a factor of 5–10 across 71 total observations ([Roth et al. 2016](#)); there is a correlation with Europa’s distance from the jovian plasma sheet, although there is significant variability between individual exposures as well as between observations at similar plasma sheet locations. There is no indication that there is a difference in brightness between sunlight and eclipse.

Our individual integrations have sufficient signal-to-noise in the  $6300/6364 \text{ \AA}$  emission that we can analyze the changes in the aurora through each eclipse, during which the plasma sheet distance is changing but longer-timescale variations in either Europa’s atmosphere or the plasma conditions do not factor in. Figure 7 shows the brightness of the  $O(^1D)$  transition, the sum of the  $6300$  and  $6364 \text{ \AA}$  lines, as a function of plasma sheet distance (as defined in [Phipps & Bagenal 2021](#)) during each observation. There is an apparent correlation with plasma sheet distance on 2021-07-16 and 2021-06-21, although we note that there is no apparent correlation on 2021-05-20, and even when present the scatter is significant and the correlation reverses slightly right at the equator. We fit a model of the form  $B(z) = B_0 e^{-(z/H)^2}$  where  $B_0$  is the brightness

as Europa is crossing the centrifugal equator of the plasma sheet (Phipps & Bagenal 2021);  $z$  is the absolute-value distance from plasma sheet in  $R_J$ , and  $H$  is the scale height (Hill et al. 1974; Roth et al. 2016). The free parameters are  $B_0$  and  $H$ , and the best-fit model is shown on Figure 7. The best-fit scale height of  $1.67 R_J$  is in the vicinity of the scale height of  $1.6 R_J$  found for the UV aurora (Roth et al. 2016), and the plasma torus scale height at Europa’s orbit of  $1.7 R_J$  from the model of Bagenal & Delamere (2011).

The UV and optical observations thus collectively demonstrate that Europa’s auroral brightness correlates with magnetic latitude, although there is large scatter about this correlation and other sources of variability may dominate on timescales of minutes to days. We note that Io’s aurora also show a factor of  $\sim 3$  variability even at a given plasma sheet location (Oliveresen et al. 2001; Roth et al. 2014b; Schmidt et al. in press), and that this is indeed expected based on observed variations in the electron density (Bagenal et al. 2015).

### 4.3. Callisto

Callisto’s atmosphere is the most poorly understood of the Galilean satellites. The presence of an ionosphere at Callisto was indicated by *Galileo* from the plasma density measured during Callisto flyby (Gurnett et al. 2000) and from radio occultation observations (Kliore et al. 2002). Under the assumption of a predominantly  $O_2$  atmosphere (which is supported by modeling work by Liang et al. (2005)), the radio occultation measurements were used to infer an  $O_2$  column density of  $4 \times 10^{16} \text{ cm}^{-2}$  (Kliore et al. 2002). However, the ionosphere was only detected on the sunlit trailing hemisphere, which is the side impacted by Jupiter’s co-rotating plasma, and not on the sunlit leading hemisphere. It was also denser on the sunlit than on the night side of Callisto’s terminator, suggesting that photons play a role in producing it. Kliore et al. (2002) hypothesized that the atmosphere is generated by sputtering, but it’s been suggested that the presence of the ionosphere should divert plasma around Callisto (Strobel et al. 2002). If this is the case, it may be that sputtering on the night side generates the atmosphere, which becomes ionized by photo-electrons when it moves into sunlight.

The first detection of Callisto’s aurora were made with HST/COS of the 1304 and 1356 Å emission lines, in sunlight on the leading/Jupiter-facing hemisphere (Cunningham et al. 2015). The observed brightnesses of  $3.3 \pm 2.8$  and  $3.2 \pm 1.6 R$  for the two emissions respectively correspond to an  $O_2$  column density of  $4 \times 10^{15} \text{ cm}^{-2}$  assuming excitation by photo-electrons. The authors argue that photo- rather than magnetospheric electrons are exciting the emissions, on the basis of the fact that photo-electron-excited emission is modeled to be  $10\times$  brighter, assuming the magnetospheric electrons penetrate to the atmosphere at all instead of being diverted around Callisto (Cunningham et al. 2015). This atmospheric density is  $5\times$  higher than the  $CO_2$  column density of  $8 \times 10^{14} \text{ cm}^{-2}$  derived from a *Galileo* off-limb airglow measurement (Carlson 1999), but  $10\times$  lower than the trailing hemisphere  $O_2$  density inferred from the ionospheric measurements.

We present the first detection of Callisto’s optical aurora from 2021-07-04, specifically the O I emissions at 6300 and 6364 Å with brightnesses of  $6.1 \pm 1.7 R$  and  $3.3 \pm 1.2 R$  respectively. Assuming a purely  $O_2$  atmosphere, these emissions correspond to a column density of  $(4.0 \pm 0.9) \times 10^{15} \text{ cm}^{-2}$ , which is identical to the column density inferred from past UV observations, although our derived column density depends on the assumed electron energies and densities at Callisto, which are poorly constrained at the current time and likely variable. The UV observations were made in sunlight, and the derived column density were based on the assumption that the aurora were primarily excited by photo-electrons rather than magnetospheric electrons. Our observations were made in eclipse and the detected emissions therefore must be excited by magnetospheric electrons, removing this ambiguity in interpretation. The match between our column density and that inferred from the past UV data may support the interpretation of the excitation mechanism for the UV aurora. However, the large uncertainty on the electron density, and the unknown variability

of Callisto's atmosphere and the electron density at Callisto's orbit, prevent firm conclusions. Assuming a purely  $O_2$  atmosphere and excitation by magnetospheric electrons alone, our measured optical emissions would correspond to emission of 0.5 R at 1304 Å and 1.2 R at 1356 Å (see Table 6). These values are lower than the UV aurora measurements of  $3.3 \pm 2.8$  R and  $3.2 \pm 1.6$  R, which suggests photoelectrons are indeed needed to excite the observed UV emissions, although the measurements are still consistent within 1–2 $\sigma$  with magnetospheric electron excitation due to the large uncertainties. In addition, the column densities inferred from aurora for the leading/subjovian hemispheres are an order of magnitude lower than the estimate from radio occultation for the trailing hemisphere of  $4 \times 10^{16}$  cm<sup>-2</sup> (Cunningham et al. 2015; Kliore et al. 2002), which could be due to enhanced atmospheric generation via sputtering on the trailing hemisphere if confirmed by measurements of both hemispheres using the same technique.

The detection of combined 6300 and 6364 Å emission at 9.4 R along with the upper limit on 5577 Å of 2 R places a lower limit on the  $O(^1D)/O(^1S)$  ratio of 4.75. This rules out  $H_2O$  as the dominant parent molecule, as it would produce an emission ratio of 1.2 (see Table 5). Atomic O was previously ruled out as the dominant parent species due to an early non-detection of 1304 Å, which is produced in part by resonant scattering (Strobel et al. 2002).  $CO_2$  is known to be present in Callisto's atmosphere, but the  $CO_2$  column density of  $1.1 \times 10^{16}$  cm<sup>-2</sup> that would be required to produce our measured auroral emissions is two orders of magnitude higher than the detected  $CO_2$  atmosphere (Carlson 1999). We conclude that molecular  $O_2$  is the most plausible parent molecule for the aurora we observe at Callisto.

## 5. CONCLUSIONS

We present new detections of oxygen auroral emissions at the icy Galilean satellites Europa, Ganymede and Callisto. At Europa we detect emission at 6300/6364, 5577 and 7774 Å, including the first detection of emissions at the latter two of these wavelengths. At Ganymede we present the first detections of aurora at any optical wavelength, including measurements at 6300/6364, 5577, 7774 and 8446 Å. At Callisto we present the first detection at any wavelength of aurora that must be excited by magnetospheric electrons, via a detection of the 6300/6364 Å lines. Upper limits are presented for oxygen lines when not detected, and for hydrogen  $H\alpha$  in all observations.

The emissions from Europa and Ganymede are fit with atmospheres that are permitted to contain O,  $O_2$  and  $H_2O$ . The best-fit atmosphere for Europa is predominantly  $O_2$  with a column density of  $4.1 \pm 0.1 \times 10^{14}$  cm<sup>-2</sup>, and we find weak evidence for  $H_2O$  at a column density of  $1.2 \pm 0.5 \times 10^{14}$  cm<sup>-2</sup>. The best-fit atmosphere for Ganymede is exclusively  $O_2$  at a column density of  $4.7 \pm 0.1 \times 10^{14}$  cm<sup>-2</sup>; an upper limit of  $3 \times 10^{13}$  cm<sup>-2</sup> is placed on both atomic O and  $H_2O$ . These data place strong constraints on  $H_2O$  abundance because of the unique sensitivity of the 5577 Å and  $H\alpha$  emissions to the presence of water.

Callisto's aurora indicate an  $O_2$  column density of  $4.0 \pm 0.9 \times 10^{15}$  cm<sup>-2</sup> for our adopted electron properties. This matches the column density inferred from past UV observations (Cunningham et al. 2015), even though the UV aurora were attributed to photoelectron excitation whereas we observe emissions in eclipse that must be excited by magnetospheric electrons.

These data collectively demonstrate the power of the optical aurora in providing a collection of emission lines that can clearly differentiate between parent species and provide robust constraints on atmospheric make-up. The recently-launched *James Webb Space Telescope* will cover the wavelengths of the majority of the transitions presented here and may provide new insight into not just the strength of the aurora but their spatial variations across the satellites.



Support for this work was provided by NASA through grant to program HST-GO-15425 from the Space Telescope Science Institute, which is operated by the Associations of Universities for Research in Astronomy, Incorporated, under NASA contract NAS5-26555. We also gratefully acknowledge support from the NASA Solar System Observations program via grants 80NSSC22K0954 and 80NSSC21K1138. The data presented herein were obtained at the W. M. Keck Observatory, which is operated as a scientific partnership among the California Institute of Technology, the University of California and the National Aeronautics and Space Administration. The Observatory was made possible by the generous financial support of the W. M. Keck Foundation. The authors wish to recognize and acknowledge the very significant cultural role and reverence that the summit of Maunakea has always had within the indigenous Hawaiian community. We are most fortunate to have the opportunity to conduct observations from this mountain.

*Facilities:* Keck/HIRES

**Table 4.** Emission rate coefficients for Europa, Ganymede and Callisto.

		Parent Species [ $\times 10^{-10} \text{ cm}^3 \text{ s}^{-1}$ ]											
		Europa				Ganymede				Callisto			
	Wavelength [ $\text{\AA}$ ]	O	O <sub>2</sub>	H <sub>2</sub> O	CO <sub>2</sub>	O	O <sub>2</sub>	H <sub>2</sub> O	CO <sub>2</sub>	O	O <sub>2</sub>	H <sub>2</sub> O	CO <sub>2</sub>
O( <sup>1</sup> S)	5577	4.8	4.4	2.5	40	2.4	11	7.6	85	4.4	6.7	4.2	57
O( <sup>1</sup> D)	6300 + 6364	33	118	3.1	—	7.9	200	9.4	—	23	156	5.2	—
O( <sup>3</sup> S)	1304	37	5.9	0.33	1.1	50	14	1.3	3.8	37	5.9	0.3	1.1
O( <sup>5</sup> S)	1356	4.6	13	0.082	1.0	1.1	32	0.33	3.9	4.6	13	0.08	1.0
O(3p <sup>3</sup> P)	8446	9.8	3.6	0.40	—	7.2	9.9	1.4	—	9.8	3.6	0.4	—
O(3p <sup>5</sup> P)	7774	2.0	6.8	0.20	—	0.54	21	0.53	—	2.0	6.8	0.2	—
Ly- $\alpha$	1216	—	—	9.3	—	—	—	33	—	—	—	9.3	—
H $\alpha$	6563	—	—	5.0	—	—	—	15	—	—	—	5.0	—

**Table 5.** Modeled emission ratios for Europa, Ganymede and Callisto.

		Parent Species											
		Europa				Ganymede				Callisto			
Ratio	Wavelengths [ $\text{\AA}$ ]	O	O <sub>2</sub>	H <sub>2</sub> O	CO <sub>2</sub>	O	O <sub>2</sub>	H <sub>2</sub> O	CO <sub>2</sub>	O	O <sub>2</sub>	H <sub>2</sub> O	CO <sub>2</sub>
Ly- $\alpha$ /H- $\alpha$	1216/6563	—	—	1.9	—	—	—	2.1	—	—	—	2.0	—
O( <sup>1</sup> D)/H- $\alpha$	(6300 + 6364)/6563	—	—	0.61	—	—	—	0.61	—	—	—	0.60	—
O( <sup>1</sup> D)/O( <sup>1</sup> S)	(6300 + 6364)/5577	6.7	27	1.2	—	3.3	19	1.2	—	5.2	23	1.2	—
O( <sup>1</sup> D)/O( <sup>5</sup> S)	(6300 + 6364)/1356	7.1	9.2	37	—	7.3	6.3	29	—	7.0	7.8	32	—
O( <sup>1</sup> D)/O( <sup>3</sup> S)	(6300 + 6364)/1304	0.89	20	9.3	—	0.16	14	7.2	—	0.5	17	8	—
O( <sup>1</sup> D)/O(3p <sup>5</sup> P)	(6300 + 6364)/7774	16	17	15	—	15	9.6	18	—	15	13	15	—
O( <sup>1</sup> D)/O(3p <sup>3</sup> P)	(6300 + 6364)/8446	3.3	33	7.6	—	1.1	20	6.9	—	2	27	7	—
O( <sup>5</sup> S)/O( <sup>3</sup> S)	1356/1304	0.11	2.2	0.25	0.91	0.022	2.2	0.25	1.0	0.07	2.2	0.25	0.97
O( <sup>5</sup> S)/O( <sup>1</sup> S)	1356/5577	0.94	2.9	0.033	0.026	0.046	2.9	0.043	0.046	0.74	3.0	0.038	0.034

## APPENDIX

## A. EMISSION MODEL

## B. BEST-FIT MODEL PROPERTIES

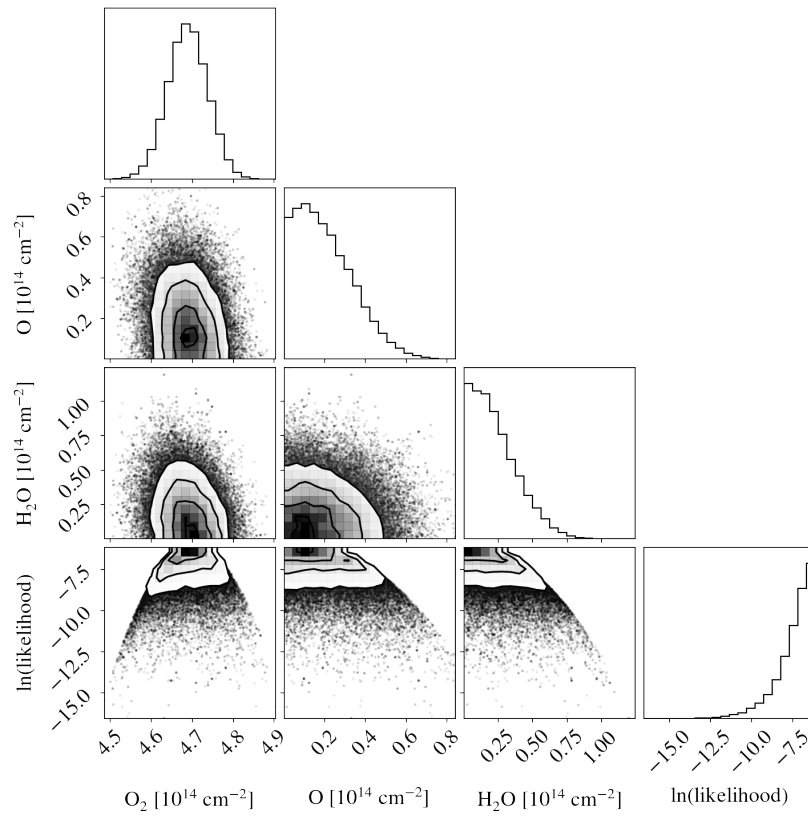


**Figure 8.** Example MCMC output showing the individual and joint posterior distributions for the column densities of the three atmospheric species, based on the measurements and upper limits for the Ganymede average case. In the fits, the electron energies and densities are fixed at the values described in the text, and the column densities of the three species are the free parameters in the fit.

**Table 6.** Best-fit models for Europa, Ganymede, and Callisto.<sup>a</sup>

Date	Column Density			Aurora Surface Brightness							
	O <sub>2</sub>	O	H <sub>2</sub> O	6300 + 6364 Å	5577 Å	7774 Å	8446 Å	6563 Å	1304 Å	1356 Å	1216 Å
	[× 10 <sup>14</sup> cm <sup>-2</sup> ]			O( <sup>1</sup> D)	O( <sup>1</sup> S)	O(3p <sup>3</sup> P)	O(3p <sup>3</sup> P)	H-α	O( <sup>3</sup> S)	O( <sup>5</sup> S)	Ly-α
<b>Europa</b>											
2021-05-20											
<i>Result w/Uncertainties</i>	4.0 ± 0.1	< 0.4	< 0.9	—	—	—	—	—	—	—	—
<i>Max-Likelihood Model</i>	4.0	0.0003	0.73	763	31	44	24	6	38	83	11
<i>Measured Brightnesses</i>	—	—	—	763 ± 16	37 ± 4	30 ± 15	< 22	< 12	—	—	—
2021-06-21											
<i>Result w/Uncertainties</i>	3.7 ± 0.2	1.8 ± 0.8	< 0.8	—	—	—	—	—	—	—	—
<i>Max-Likelihood Model</i>	3.7	1.8	0.16	788	40	46	49	1.2	137	89	2.3
<i>Measured Brightnesses</i>	—	—	—	789 ± 13	42 ± 5	< 40	< 80	< 12	—	—	—
2021-07-16											
<i>Result w/Uncertainties</i>	3.7 ± 0.2	< 1.2	< 1.1	—	—	—	—	—	—	—	—
<i>Max-Likelihood Model</i>	3.7	0.37	0.35	717	30	42	27	3	56	79	5
<i>Measured Brightnesses</i>	—	—	—	717 ± 16	35 ± 8	< 60	< 60	< 18	—	—	—
Average <sup>b</sup>											
<i>Result w/Uncertainties</i>	4.1 ± 0.1	< 0.1	1.2 ± 0.5	—	—	—	—	—	—	—	—
<i>Max-Likelihood Model</i>	4.1	0.02	1.2	777	34	45	25	10	40	84	18
<i>Measured Brightnesses</i>	—	—	—	776 ± 10	40 ± 3	30 ± 15	< 22	< 12	40 ± 4	80 ± 8	—
<b>Ganymede</b>											
1998-11-15											
<i>Result w/Uncertainties</i>	4.5 ± 0.1	< 3	< 0.6	—	—	—	—	—	—	—	—
<i>Max-Likelihood Model</i>	4.5	0.001	0.004	182	10	19	9	0	13	29	0
<i>Measured Brightnesses</i>	—	—	—	181.9 ± 3.4	9.2 ± 1.6	—	—	< 6	—	—	—
2018-06-15											
<i>Result w/Uncertainties</i>	3.2 ± 0.3	< 8	16 ± 3	—	—	—	—	—	—	—	—
<i>Max-Likelihood Model</i>	3.2	2.7	16	164	33	16	15	50	40	22	108
<i>Measured Brightnesses</i>	—	—	—	163 ± 9	41 ± 4	< 26	< 20	< 30	—	—	—
2021-06-08											
<i>Result w/Uncertainties</i>	4.8 ± 0.1	< 0.8	< 0.5	—	—	—	—	—	—	—	—
<i>Max-Likelihood Model</i>	4.8	0.005	0.45	193	11	20	10	1	14	31	3
<i>Measured Brightnesses</i>	—	—	—	192.6 ± 1.8	12.5 ± 0.6	20 ± 2	7.3 ± 1.4	< 1.8	—	—	—
Average <sup>b</sup>											
<i>Result w/Uncertainties</i>	4.7 ± 0.1	< 0.3	< 0.3	—	—	—	—	—	—	—	—
<i>Max-Likelihood Model</i>	4.7	0.12	0.04	188	10	20	10	0.1	15	30	0.3
<i>Measured Brightnesses</i>	—	—	—	187 ± 2	11 ± 1	20 ± 2	7.3 ± 1.4	< 2	15 ± 2	36 ± 2	—
<b>Callisto</b>											
2021-07-04											
<i>Result w/Uncertainties</i>	40 ± 9	—	—	9.3	0.4	0.7	0.3	0	0.5	1.2	0.3
<i>Measured Brightnesses</i>	—	—	—	9.4 ± 2.1	< 2	< 8	< 4	< 3	—	—	—

<sup>a</sup>Our reported best-fit model with uncertainties is given under the heading “Result w/Uncertainties”. However, because the column densities are often upper limits, we also reported the single model that maximizes the likelihood function along with the auroral surface brightnesses of that model.

<sup>b</sup>Average auroral brightness are averaged over values from this work and from the literature (de Kleer & Brown 2018, 2019; Roth et al. 2016).

## REFERENCES

- Ajello, J. M. 1971, *JChPh*, 55, 3169,  
doi: [10.1063/1.1676564](https://doi.org/10.1063/1.1676564)
- Alday, J., Roth, L., Ivchenko, N., et al. 2017,  
*Planet. Space Sci.*, 148, 35,  
doi: [10.1016/j.pss.2017.10.006](https://doi.org/10.1016/j.pss.2017.10.006)
- Bagenal, F., & Delamere, P. A. 2011, *Journal of Geophysical Research (Space Physics)*, 116, A05209, doi: [10.1029/2010JA016294](https://doi.org/10.1029/2010JA016294)
- Bagenal, F., & Dols, V. 2020, *Journal of Geophysical Research (Space Physics)*, 125, e27485, doi: [10.1029/2019JA027485](https://doi.org/10.1029/2019JA027485)
- Bagenal, F., Sidrow, E., Wilson, R. J., et al. 2015,  
*Icarus*, 261, 1, doi: [10.1016/j.icarus.2015.07.036](https://doi.org/10.1016/j.icarus.2015.07.036)
- Beenakker, C. I. M., Heer, F. J. D., Krop, H. B., & Möhlmann, G. R. 1974, *Chemical Physics*, 6, 445, doi: [10.1016/0301-0104\(74\)85028-7](https://doi.org/10.1016/0301-0104(74)85028-7)
- Belcher, J. W. 1983, in *Physics of the Jovian Magnetosphere* (Cambridge University Press), 68–105
- Belton, M. J. S., Head, J. W., I., Ingersoll, A. P., et al. 1996, *Science*, 274, 377, doi: [10.1126/science.274.5286.377](https://doi.org/10.1126/science.274.5286.377)
- Borucki, W. J., McKay, C. P., Jebens, D., Lakkaraju, H. S., & Vanajakshi, C. T. 1996, *Icarus*, 123, 336, doi: [10.1006/icar.1996.0162](https://doi.org/10.1006/icar.1996.0162)
- Bougher, S. W., Brain, D. A., Fox, J. L., et al. 2017, in *The Atmosphere and Climate of Mars*, ed. R. M. Haberle, R. T. Clancy, F. Forget, M. D. Smith, & R. W. Zurek (Cambridge University Press), 405–432, doi: [10.1017/9781139060172.014](https://doi.org/10.1017/9781139060172.014)
- Broadfoot, A. L., Belton, M. J. S., Takacs, P. Z., et al. 1979, *Science*, 204, 979, doi: [10.1126/science.204.4396.979](https://doi.org/10.1126/science.204.4396.979)
- Brown, W. L., Augustyniak, W. M., Lanzerotti, L. J., Johnson, R. E., & Evatt, R. 1980, *PhRvL*, 45, 1632, doi: [10.1103/PhysRevLett.45.1632](https://doi.org/10.1103/PhysRevLett.45.1632)
- Buton, C., Copin, Y., Aldering, G., et al. 2013, *Astronomy and Astrophysics*, 549, doi: [10.1051/0004-6361/201219834](https://doi.org/10.1051/0004-6361/201219834)
- Carberry Mogan, S. R., Tucker, O. J., Johnson, R. E., et al. 2021, *Icarus*, 368, 114597, doi: [10.1016/j.icarus.2021.114597](https://doi.org/10.1016/j.icarus.2021.114597)
- Carlson, R. W. 1999, *Science*, 283, 820, doi: [10.1126/science.283.5403.820](https://doi.org/10.1126/science.283.5403.820)
- Carlson, R. W., Bhattacharyya, J. C., Smith, B. A., et al. 1973, *Science*, 182, 53, doi: [10.1126/science.182.4107.53](https://doi.org/10.1126/science.182.4107.53)
- Cassidy, T. A., Johnson, R. E., Geissler, P. E., & Leblanc, F. 2008, *Journal of Geophysical Research: Planets*, 113, doi: <https://doi.org/10.1029/2007JE002955>
- Cassidy, T. A., Paranicas, C. P., Shirley, J. H., et al. 2013, *Planet. Space Sci.*, 77, 64, doi: [10.1016/j.pss.2012.07.008](https://doi.org/10.1016/j.pss.2012.07.008)
- Cunningham, N. J., Spencer, J. R., Feldman, P. D., et al. 2015, *Icarus*, 254, 178, doi: [10.1016/j.icarus.2015.03.021](https://doi.org/10.1016/j.icarus.2015.03.021)
- de Kleer, K., & Brown, M. E. 2018, *AJ*, 156, 167, doi: [10.3847/1538-3881/aadae8](https://doi.org/10.3847/1538-3881/aadae8)
- . 2019, *Research Notes of the American Astronomical Society*, 3, 27, doi: [10.3847/2515-5172/ab0289](https://doi.org/10.3847/2515-5172/ab0289)
- Eviatar, A., Strobel, D. F., Wolven, B. C., et al. 2001, *ApJ*, 555, 1013, doi: [10.1086/321510](https://doi.org/10.1086/321510)
- Feistel, R., & Wagner, W. 2007, *GeoCoA*, 71, 36, doi: [10.1016/j.gca.2006.08.034](https://doi.org/10.1016/j.gca.2006.08.034)
- Feldman, P. D., McGrath, M. A., Strobel, D. F., et al. 2000, *ApJ*, 535, 1085, doi: [10.1086/308889](https://doi.org/10.1086/308889)
- Foreman-Mackey, D., Hogg, D. W., Lang, D., & Goodman, J. 2013, *PASP*, 125, 306, doi: [10.1086/670067](https://doi.org/10.1086/670067)
- Goodman, J., & Weare, J. 2010, *Communications in Applied Mathematics and Computational Science*, 5, 65, doi: [10.2140/camcos.2010.5.65](https://doi.org/10.2140/camcos.2010.5.65)
- Gronoff, G., Lilensten, J., Simon, C., et al. 2008, *A&A*, 482, 1015, doi: [10.1051/0004-6361:20077503](https://doi.org/10.1051/0004-6361:20077503)
- Gulcicek, E. E., & Doering, J. P. 1987, *J. Geophys. Res.*, 92, 3445, doi: [10.1029/JA092iA04p03445](https://doi.org/10.1029/JA092iA04p03445)
- Gulcicek, E. E., Doering, J. P., & Vaughan, S. O. 1988, *J. Geophys. Res.*, 93, 5885, doi: [10.1029/JA093iA06p05885](https://doi.org/10.1029/JA093iA06p05885)
- Gurnett, D. A., Persoon, A. M., Kurth, W. S., Roux, A., & Bolton, S. J. 2000, *Geophys. Res. Lett.*, 27, 1867, doi: [10.1029/2000GL003751](https://doi.org/10.1029/2000GL003751)
- Hall, D. T., Feldman, P. D., McGrath, M. A., & Strobel, D. F. 1998, *ApJ*, 499, 475, doi: [10.1086/305604](https://doi.org/10.1086/305604)
- Hall, D. T., Strobel, D. F., Feldman, P. D., McGrath, M. A., & Weaver, H. A. 1995, *Nature*, 373, 677, doi: [10.1038/373677a0](https://doi.org/10.1038/373677a0)
- Hansell, S. A., Wells, W. K., & Hunten, D. M. 1995, *Icarus*, 117, 345, doi: [10.1006/icar.1995.1160](https://doi.org/10.1006/icar.1995.1160)
- Hill, T. W., Dessler, A. J., & Michel, F. C. 1974, *Geophys. Res. Lett.*, 1, 3, doi: [10.1029/GL001i001p00003](https://doi.org/10.1029/GL001i001p00003)



- Ip, W. H. 1996, *Icarus*, 120, 317, doi: [10.1006/icar.1996.0052](https://doi.org/10.1006/icar.1996.0052)
- Itikawa, Y. 2002, *Journal of Physical and Chemical Reference Data*, 31, 749, doi: [10.1063/1.1481879](https://doi.org/10.1063/1.1481879)
- Itikawa, Y., & Mason, N. 2005, *Journal of Physical and Chemical Reference Data*, 34, 1, doi: [10.1063/1.1799251](https://doi.org/10.1063/1.1799251)
- Johnson, R. E., Lanzerotti, L. J., & Brown, W. L. 1982, *Nuclear Instruments and Methods in Physics Research*, 198, 147, doi: [10.1016/0167-5087\(82\)90066-7](https://doi.org/10.1016/0167-5087(82)90066-7)
- Johnson, R. E., Lanzerotti, L. J., Brown, W. L., & Armstrong, T. P. 1981, *Science*, 212, 1027, doi: [10.1126/science.212.4498.1027](https://doi.org/10.1126/science.212.4498.1027)
- Johnson, R. E., Oza, A. V., Leblanc, F., et al. 2019, *SSRv*, 215, 20, doi: [10.1007/s11214-019-0582-1](https://doi.org/10.1007/s11214-019-0582-1)
- Kivelson, M. G., Bagenal, F., Kurth, W. S., et al. 2004, in *Jupiter. The Planet, Satellites and Magnetosphere*, ed. F. Bagenal, T. E. Dowling, & W. B. McKinnon, Vol. 1 (Cambridge University Press), 513–536
- Kliore, A. J., Anabtawi, A., Herrera, R. G., et al. 2002, *Journal of Geophysical Research (Space Physics)*, 107, 1407, doi: [10.1029/2002JA009365](https://doi.org/10.1029/2002JA009365)
- Kurth, W. S., Sulaiman, A. H., Hospodarsky, G. B., et al. 2022, *Geophysical Research Letters*, n/a, e2022GL098591, doi: <https://doi.org/10.1029/2022GL098591>
- Laher, R. R., & Gilmore, F. R. 1990, *Journal of Physical and Chemical Reference Data*, 19, 277, doi: [10.1063/1.555872](https://doi.org/10.1063/1.555872)
- Lanzerotti, L. J., Brown, W. L., Poate, J. M., & Augustyniak, W. M. 1978, *Geophys. Res. Lett.*, 5, 155, doi: [10.1029/GL005i002p00155](https://doi.org/10.1029/GL005i002p00155)
- Leblanc, F., Oza, A. V., Leclercq, L., et al. 2017, *Icarus*, 293, 185, doi: [10.1016/j.icarus.2017.04.025](https://doi.org/10.1016/j.icarus.2017.04.025)
- LeClair, L. R., & McConkey, J. W. 1994, *Journal of Physics B Atomic Molecular Physics*, 27, 4039, doi: [10.1088/0953-4075/27/17/026](https://doi.org/10.1088/0953-4075/27/17/026)
- Liang, M.-C., Lane, B. F., Pappalardo, R. T., Allen, M., & Yung, Y. L. 2005, *Journal of Geophysical Research (Planets)*, 110, E02003, doi: [10.1029/2004JE002322](https://doi.org/10.1029/2004JE002322)
- Lorenz, R. D., Imai, M., Takahashi, Y., et al. 2019, *Geophysical Research Letters*, 46, 7955, doi: <https://doi.org/10.1029/2019GL083311>
- Marconi, M. L. 2007, *Icarus*, 190, 155, doi: [10.1016/j.icarus.2007.02.016](https://doi.org/10.1016/j.icarus.2007.02.016)
- McCully, C., Crawford, S., Kovacs, G., et al. 2018, *Astro-SCRAPPY*. <https://zenodo.org/record/1482019>
- McGrath, M. A., Jia, X., Retherford, K., et al. 2013, *Journal of Geophysical Research (Space Physics)*, 118, 2043, doi: [10.1002/jgra.50122](https://doi.org/10.1002/jgra.50122)
- Molyneux, P. M., Nichols, J. D., Bannister, N. P., et al. 2018, *Journal of Geophysical Research (Space Physics)*, 123, 3777, doi: [10.1029/2018JA025243](https://doi.org/10.1029/2018JA025243)
- Mumma, M. J., Stone, E. J., Borst, W. L., & Zipf, E. C. 1972, *JChPh*, 57, 68, doi: [10.1063/1.1678019](https://doi.org/10.1063/1.1678019)
- Oliversen, R. J., Scherb, F., Smyth, W. H., et al. 2001, *J. Geophys. Res.*, 106, 26183, doi: [10.1029/2000JA002507](https://doi.org/10.1029/2000JA002507)
- Oza, A. V., Johnson, R. E., & Leblanc, F. 2018, *Icarus*, 305, 50, doi: [10.1016/j.icarus.2017.12.032](https://doi.org/10.1016/j.icarus.2017.12.032)
- Oza, A. V., Leblanc, F., Johnson, R. E., et al. 2019, *Planet. Space Sci.*, 167, 23, doi: [10.1016/j.pss.2019.01.006](https://doi.org/10.1016/j.pss.2019.01.006)
- Pavlov, A. V., & Berrington, K. A. 1999, *Annales Geophysicae*, 17, 919, doi: [10.1007/s00585-999-0919-2](https://doi.org/10.1007/s00585-999-0919-2)
- Phipps, P., & Bagenal, F. 2021, *Journal of Geophysical Research (Space Physics)*, 126, e28713, doi: [10.1029/2020JA028713](https://doi.org/10.1029/2020JA028713)
- Plainaki, C., Milillo, A., Mura, A., et al. 2013, *Planet. Space Sci.*, 88, 42, doi: [10.1016/j.pss.2013.08.011](https://doi.org/10.1016/j.pss.2013.08.011)
- Roth, L. 2021, *Geophys. Res. Lett.*, 48, e94289, doi: [10.1029/2021GL094289](https://doi.org/10.1029/2021GL094289)
- Roth, L., Ivchenko, N., Gladstone, G. R., et al. 2021, *Nature Astronomy*, 5, 1043, doi: [10.1038/s41550-021-01426-9](https://doi.org/10.1038/s41550-021-01426-9)
- Roth, L., Retherford, K. D., Saur, J., et al. 2014a, *Proceedings of the National Academy of Science*, 111, E5123, doi: [10.1073/pnas.1416671111](https://doi.org/10.1073/pnas.1416671111)
- Roth, L., Saur, J., Retherford, K. D., Feldman, P. D., & Strobel, D. F. 2014b, *Icarus*, 228, 386, doi: [10.1016/j.icarus.2013.10.009](https://doi.org/10.1016/j.icarus.2013.10.009)
- Roth, L., Saur, J., Retherford, K. D., et al. 2016, *Journal of Geophysical Research (Space Physics)*, 121, 2143, doi: [10.1002/2015JA022073](https://doi.org/10.1002/2015JA022073)
- Saur, J., Strobel, D. F., & Neubauer, F. M. 1998, *J. Geophys. Res.*, 103, 19947, doi: [10.1029/97JE03556](https://doi.org/10.1029/97JE03556)
- Saur, J., Duling, S., Roth, L., et al. 2015, *Journal of Geophysical Research (Space Physics)*, 120, 1715, doi: [10.1002/2014JA020778](https://doi.org/10.1002/2014JA020778)
- Schmidt, C., Sharov, M., de Kleer, K., et al. in press, *PSJ*
- Schulman, M. B., Sharpton, F. A., Chung, S., Lin, C. C., & Anderson, L. W. 1985, *PhRvA*, 32, 2100, doi: [10.1103/PhysRevA.32.2100](https://doi.org/10.1103/PhysRevA.32.2100)

- Shemansky, D. E., Yung, Y. L., Liu, X., et al. 2014, *The Astrophysical Journal*, 797, 84, doi: [10.1088/0004-637x/797/2/84](https://doi.org/10.1088/0004-637x/797/2/84)
- Shematovich, V. I., Johnson, R. E., Cooper, J. F., & Wong, M. C. 2005, *Icarus*, 173, 480, doi: [10.1016/j.icarus.2004.08.013](https://doi.org/10.1016/j.icarus.2004.08.013)
- Sittler, E. C., & Strobel, D. F. 1987, *J. Geophys. Res.*, 92, 5741, doi: [10.1029/JA092iA06p05741](https://doi.org/10.1029/JA092iA06p05741)
- Slanger, T. G., Cosby, P. C., Huestis, D. L., & Meier, R. R. 2004, *Journal of Geophysical Research (Space Physics)*, 109, A10309, doi: [10.1029/2004JA010556](https://doi.org/10.1029/2004JA010556)
- Smyth, W. H., & Marconi, M. L. 2006, *Icarus*, 181, 510, doi: [10.1016/j.icarus.2005.10.019](https://doi.org/10.1016/j.icarus.2005.10.019)
- Streit, G. E., Howard, C. J., Schmeltekopf, A. L., Davidson, J. A., & Schiff, H. I. 1976, *The Journal of Chemical Physics*, 65, 4761, doi: [10.1063/1.432930](https://doi.org/10.1063/1.432930)
- Strobel, D. F., Saur, J., Feldman, P. D., & McGrath, M. A. 2002, *ApJL*, 581, L51, doi: [10.1086/345803](https://doi.org/10.1086/345803)
- Teolis, B. D., Plainaki, C., Cassidy, T. A., & Raut, U. 2017, *Journal of Geophysical Research (Planets)*, 122, 1996, doi: [10.1002/2017JE005285](https://doi.org/10.1002/2017JE005285)
- van Dokkum, P. G. 2001, *Publications of the Astronomical Society of the Pacific*, 113, 1420, doi: [10.1086/323894](https://doi.org/10.1086/323894)
- Vogt, S. S., Allen, S. L., Bigelow, B. C., et al. 1994, in *Society of Photo-Optical Instrumentation Engineers (SPIE) Conference Series*, Vol. 2198, *Instrumentation in Astronomy VIII*, ed. D. L. Crawford & E. R. Craine, 362, doi: [10.1117/12.176725](https://doi.org/10.1117/12.176725)
- Vorbürger, A., Fatemi, S., Galli, A., et al. 2022, *Icarus*, 375, 114810, doi: [10.1016/j.icarus.2021.114810](https://doi.org/10.1016/j.icarus.2021.114810)
- Vorbürger, A., & Wurz, P. 2021, *Journal of Geophysical Research (Space Physics)*, 126, e29690, doi: [10.1029/2021JA029690](https://doi.org/10.1029/2021JA029690)
- Wiese, W. L., Fuhr, J. R., & Deters, T. M. 1996, *Journal of Physical and Chemical Reference Data*, Monograph No. 7
- Wolff, R. S., & Mendis, D. A. 1983, *J. Geophys. Res.*, 88, 4749, doi: [10.1029/JA088iA06p04749](https://doi.org/10.1029/JA088iA06p04749)
- Woodman, J. H., Cochran, W. D., & Slavsky, D. B. 1979, *Icarus*, 37, 73, doi: [10.1016/0019-1035\(79\)90116-7](https://doi.org/10.1016/0019-1035(79)90116-7)
- Yung, Y. L., & McElroy, M. B. 1977, *Icarus*, 30, 97, doi: [10.1016/0019-1035\(77\)90124-5](https://doi.org/10.1016/0019-1035(77)90124-5)